Protein kinase D1 deletion in adipocytes enhances energy dissipation and protects against adiposity

Mona C. Löffler[1], Alexander E. Mayer[1], Jonathan Trujillo Viera[1], Angel Loza Valdes[1], Rabih El-Merahbi[1], Carsten P. Ade[2], Till Karwen[1], Werner Schmitz[2], Anja Slotta[1], Manuela Erk[1], Sudha Janaki-Raman[2], Nuria Matesanz[3], Jorge L. Torres[4], Miguel Marcos[4,5], Guadalupe Sabio[3], Martin Eilers[2], Almut Schulze[2], and Grzegorz Sumara[1*]

[1]Rudolf Virchow Center for Experimental Biomedicine, University of Würzburg, Josef-Schneider-Str. 2, Haus D15, 97080 Würzburg, Germany

[2]Theodor Boveri Institute, Biocenter, University of Würzburg, Am Hubland, 97074 Würzburg, Germany

[3]Centro Nacional de Investigaciones Cardiovasculares Carlos III (CNIC), C/ Melchor Fernández Almagro 3, 28029 Madrid, Spain

[4]Department of Internal Medicine University Hospital of Salamanca-IBSAL Paseo de San Vicente 58, 37007 Salamanca, Spain

[5]Department of Medicine, University of Salamanca, Department of Internal Medicine University Hospital of Salamanca-IBSAL Paseo de San Vicente 58, 37007 Salamanca, Spain

* Correspondence should be addressed to Grzegorz Sumara: Rudolf Virchow Center for Experimental Biomedicine, University of Würzburg, Josef-Schneider-Straße 2, Haus D15, 97080 Würzburg, Germany. Phone: +49 931 31-89263, Email: grzegorz.sumara@uni-wuerzburg.de

Running title:

PKD1 promotes obesity and diabetes

Keywords:

AMP-activated protein kinase (AMPK)/Beige adipocytes/β3 adrenergic receptor (ADRB3)/C/EBP/Protein kinase D1 (PKD1)

Abstract

Nutrient overload in combination with decreased energy dissipation promotes obesity and diabetes. Obesity results in a hormonal imbalance, which among others, activates G-protein coupled receptors utilizing diacylglycerol (DAG) as secondary messenger. Protein kinase D1 (PKD1) is a DAG effector which integrates multiple nutritional and hormonal inputs, but its physiological role in adipocytes is unknown. Here, we show that PKD1 promotes lipogenesis and suppresses mitochondrial fragmentation, biogenesis, respiration, and energy dissipation in an AMP-activated protein kinase (AMPK)-dependent manner. Moreover, mice lacking PKD1 in adipocytes are resistant to diet-induced obesity due to elevated energy expenditure. Beiging of adipocytes promotes energy expenditure and counteracts obesity. Consistently, deletion of PKD1 promotes expression of the β3-adrenergic receptor (ADRB3) in a CCAAT/enhancer-binding protein (C/EBP)-α and δ-dependent manner, which leads to the elevated expression of beige markers in adipocytes and subcutaneous adipose tissue. Finally, deletion of PKD1 in adipocytes improves insulin sensitivity and ameliorates liver steatosis. Thus, loss of PKD1 in adipocytes increases energy dissipation by several complementary mechanisms and might represent an attractive strategy to treat obesity and its related complications.

Introduction

Persistent imbalance between energy intake and dissipation results in obesity, insulin resistance and can lead to the development of type 2 diabetes (T2D) and liver steatosis (Rosen & Spiegelman, 2006, Spiegelman & Flier, 2001). Recent studies indicate that white adipocytes, which were previously seen only as a storage compartment of the organism, present a high degree of plasticity and can acquire a molecular machinery, which allows them to dissipate energy in the form of heat. This process is often referred to as browning or beiging of white adipose tissue. Importantly, strategies to increase energy dissipation by adipocytes recently became central for the development of new anti-obesity therapies (Kajimura & Saito, 2014, Kajimura, Spiegelman et al., 2015, Kazak, Chouchani et al., 2015, Muller, Lee et al., 2013). On the molecular level, beige or brite adipocytes are characterized by the high mitochondrial content and expression of genes, which decouple the proton gradient from ATP production (Kajimura et al., 2015). Moreover, recent studies indicate that the induction of mitochondrial fragmentation also promotes decoupling activity in adipocytes, which protects mice from the development of diabetes and fatty liver disease (Tol, Ottenhoff et al., 2016, Wikstrom, Mahdaviani et al., 2014).

Obesity-related metabolic overload leads to hormonal imbalance which promotes the activity of multiple cell surface receptors including G protein-coupled receptors, which utilize diacylglycerol (DAG) as a secondary messenger (Samuel & Shulman, 2012). The impact of DAG-evoked signaling on the adipocyte function remains poorly characterized. Protein kinase D (PKD) isoforms (PKD1, 2, and 3) are DAG and protein kinase C (PKC) effectors that integrate various nutritional and hormonal inputs and have been shown to be implicated in the regulation of multiple fundamental biological processes (Rozengurt, 2011). Previous studies implicated PKD1 in the regulation of muscle differentiation, pathophysiological heart remodeling, immune response, carcinogenesis, insulin secretion, actin remodeling, trans-Golgi network dynamics, cell proliferation, and cell migration (Bergeron, Ghislain et al., 2018,

Ferdaoussi, Bergeron et al., 2012, Fielitz, Kim et al., 2008, Gehart, Goginashvili et al., 2012, Goginashvili, Zhang et al., 2015, Ittner, Block et al., 2012, Kim, Fielitz et al., 2008, Matthews, Liu et al., 2006, Rozengurt, 2011, Steiner, Ivison et al., 2010, Sumara, Formentini et al., 2009) However, the impact of PKD1 on energy dissipation and its physiological role in adipose tissue remains unknown.

Here, we show that the ablation of PKD1 in murine adipocytes results in a significant decrease of lipogenesis rate and accumulation of triglycerides (TG). At the same time, PKD1 deficiency results in an increased respiration and energy dissipation caused by mitochondrial fragmentation. On the other hand, adipocytes expressing a constitutive active form of PKD1 present a reversed phenotype. Importantly, mice lacking PKD1 specifically in adipocytes are resistant to diet-induced obesity and T2D due to an elevated mitochondrial content and high expression of genes promoting energy dissipation in white adipocytes. Finally, our results indicate that PKD1 regulates adipocyte function primarily in an AMPK-dependent manner. Taken together, our data demonstrate that PKD1 suppresses energy dissipation and drives lipogenesis and adiposity in animals. Therefore, ablation of PKD1 action in adipocytes might represent an attractive strategy to ameliorate obesity and T2D in the future.

Results

PKD1 promotes triglyceride accumulation in adipocytes

PKD1 is activated in response to the stimulation of multiple cell surface receptors, which utilize DAG as a secondary messenger (Rozengurt, 2011). Indeed, DAG can promote activation of PKD1 in undifferentiated 3T3L1 cells as well as in 3T3L1 cells, which were differentiated into adipocytes (Fig EV1A). Adiposity is associated with an increased rate of lipogenesis in all types of adipocytes. This raises the possibility that DAG accumulates in adipose tissue of obese mice. We measured steady state levels of DAG in white and brown adipose tissue of lean mice fed normal chow diet (ND) and obese mice fed high fat diet (HFD). However, diet regiment and degree of obesity did not change the DAG levels in both tissues (Fig EV1B). Factors secreted by the peripheral nervous system (β-adrenergic agonists) together with endocrine factors like insulin and gut-derived serotonin as well as auto- and paracrine factors (adenosines; ADP and ATP) regulate adipocyte function (El-Merahbi, Loffler et al., 2015, Sumara, Sumara et al., 2012, Tozzi & Novak, 2017, Zechner, Zimmermann et al., 2012). We showed that among all of these factors only extracellular purines (ADP and ATP) robustly and specifically activates PKD1 in white adipocytes (Fig EV1C-F). In brown-like adipocytes extracellular purines also can activate PKD1. However, stimulation of these cells with insulin and serotonin also increases activity of PKD1 (Fig EV1G-I).

This result prompted us to investigate the impact of PKD1 on adipocyte function. Efficient shRNA-mediated PKD1 knockdown in 3T3L1 cells (Fig S1A) led to a significant decrease in TG accumulation after 10 days of differentiation as compared to corresponding control cells (Fig 1A and B). Conversely, over-expression of constitutive active form of PKD1 (PKD1ca) in differentiated 3T3L1 cells (Fig S1B) resulted in an increased accumulation of TG compared to control cells (Fig 1C and D).

To corroborate these findings, we generated mice lacking PKD1 specifically in adipocytes by using PKD1 floxed (PKD1f/f) mice (Fielitz et al., 2008) and a mouse strain expressing Cre

recombinase under the control of the adiponectin promoter (Eguchi, Wang et al., 2011). We confirmed efficiency and specificity of PKD1 deletion in these mice on protein and mRNA levels (Fig S1C-F). None of the other two isoforms of PKD were affected by this deletion, neither in PKD1 depleted primary cells, nor in the different depots of adipose tissue (Fig S1G and H). Importantly, stroma vascular cells (SVC) isolated from subcutaneous white adipose tissue (sWAT) of PKD1adipoΔ/Δ mice and differentiated into adipocytes presented markedly lower TG content than corresponding control SVC isolated from PKD1f/f mice (Fig S1I and J). Interestingly, deletion of PKD1 in SVC did not affect the protein levels of adipocyte differentiation markers. Particularly, levels of a major transcription factor defining terminal differentiation of adipocytes, PPARγ, were not changed. Similarly, levels of enzymes and structure proteins specific for adipocytes (ATGL, HSL and Perilipin) were unaffected (Fig S1K). Altogether, these data suggest that PKD1 promotes TG accumulation in adipocytes but does not regulate adipocyte differentiation markers.

PKD1 decreases mitochondrial respiration and promotes lipogenesis in adipocytes

Since PKD1 did not affect adipocyte differentiation, reduced TG accumulation in the absence of PKD1 can be caused by an increased rate of lipolysis, decreased lipogenesis, and/or enhanced rate of respiration in adipocytes. In differentiated SVC and 3T3L1 cells, the insulin-stimulated lipogenesis rate was markedly reduced in the absence of PKD1 (Fig 1E and F). Conversely, cells expressing PKD1ca generated more TG under basal and insulin-stimulated conditions (Fig 1G). However, the lipolysis rate was not altered in PKD1-deficient adipocytes (Fig S2A and B). Next, we measured the cellular respiration rate using a Seahorse analyzer. Deficiency of PKD1 in differentiated 3T3L1 cells, as well as in SVC, resulted in increased oxygen consumption rate (OCR) during basal respiration, in response to inhibition of the mitochondrial ATP-synthase by oligomycin as well as in response to FCCP, which stimulates the maximal respiration rate in cells. In response to antimycin A/rotenone (inhibitors of mitochondrial respiration), OCR was reduced in both PKD1-deficient and control adipocytes as compared to

the baseline (Fig 2A and Fig S2C). These results indicate that PKD1-deficient adipocytes display an increased mitochondrial activity and dissipation of energy. Consistently, an increased mitochondrial content was observed in PKD1-deficient adipocytes (Fig 2B). Conversely, expression of PKD1ca in 3T3L1-derived adipocytes suppressed mitochondrial decoupling activity and OCR (Fig 2C). These experiments demonstrate that PKD1 promotes lipid storage and suppresses energy dissipation in white adipocytes.

To test whether PKD1 also affects brown adipocyte function, we isolated SVC from interscapular brown adipose tissue (BAT) and differentiated them into brown adipocytes (BSVC). Of note, deletion of PKD1 in brown adipocytes suppressed the lipogenesis rate but did not affect basal respiration or decoupling activity of these cells (Fig S2D and E). Taken together, our data show that PKD1 primarily affects white adipocyte function by decreasing mitochondrial respiration and promoting lipogenesis.

PKD1 suppresses mitochondrial fragmentation

Mitochondria are highly dynamic organelles that undergo constant fusion and fission in order to maintain optimal mitochondrial bioenergetics (Twig, Hyde et al., 2008). Mitochondrial fragmentation was previously shown to support uncoupled respiration and therefore it increases energy expenditure in adipocytes (Tol et al., 2016, Wikstrom et al., 2014). Consistently, our results show that deletion of PKD1 in differentiated adipocytes increased mitochondrial fragmentation (Fig 2D and Fig S2F). On the other hand, there were more fused mitochondria in differentiated 3T3L1 cells expressing PKD1ca (Fig 2E). This indicates that PKD1 promotes mitochondrial fusion or suppresses mitochondrial fragmentation to suppress energy dissipation in adipocytes.

PKD1 regulates adipocyte function in an AMPK-dependent manner

To unravel the underlying molecular mechanism of PKD1-mediated regulation of adipocyte function we tested the activation of AMPK, which is a multi-subunit enzyme regulating a number of processes of energy homeostasis in adipocytes (Bijland, Mancini et al., 2013).

Importantly, previous studies showed that PKD1 phosphorylates AMPK alpha subunits and inactivates the kinase activity of the whole complex in muscle cells (Coughlan, Valentine et al., 2016). Interestingly, AMPK alpha phosphorylation at putative PKD1 sites (S485/S491) was reduced in the PKD1-deficient 3T3L1 cells as well as SVC and enhanced in 3T3L1 cells expressing PKD1ca, while total AMPK alpha levels remained unchanged (Fig 3A and Fig S3A and B). This result indicates that PKD1 suppresses AMPK activity in adipocytes. Consistently, phosphorylation of the classical AMPK targets, Acetyl-CoA carboxylase 1 and 2 (ACC1/ACC2) at S79/S221 (Bijland et al., 2013), was markedly enhanced in PKD1-deficient adipocytes and reduced in cells expressing PKD1ca (Fig 3A and Fig S3A and B). Similarly, phosphorylation of AMPK alpha subunit on T172 was enhanced in cells depleted from PKD1 and reduced in cells expressing PKD1ca (Fig 3A and Fig S3A and B). Consistently, activity of AMPK complex was markedly reduced in cells expressing PKD1ca and enhanced in PKD1-deficient adipocytes (Fig 3B and C). AMPK-dependent phosphorylation of ACC inhibits lipogenesis (Bijland et al., 2013) and chemical activation of AMPK signaling by AICAR in cells expressing PKD1ca (Fig S3C) reduced the lipogenesis rate to the levels observed in control cells (Fig 3D). In contrast, silencing of AMPK alpha subunits in differentiated 3T3L1 cells depleted of PKD1 (Fig S3D) increased the lipogenesis rate to the same level as seen in control cells (Fig 3E). Consistently, inhibition of AMPK activity with Compound C (CC) normalized reduced lipogenesis rate in PKD1-deficient adipose tissue expands (Fig 3F). In line with these findings, silencing of AMPK alpha subunits in adipocytes depleted from PKD1 normalized TG content (Fig S3E and F), while AICAR treatment reduced TG accumulation in cells expressing PKD1ca to the level observed in control cells (Fig 3G and H). Silencing of AMPK alpha subunits (Fig S3G) also normalized enhanced respiration of PKD1-deficient primary cells (Fig 3I), while AICAR treatment enhanced respiration of PKD1ca expressing cells to the levels observed in control adipocytes (Fig 3J). Finally, activation of AMPK in PKD1ca expressing

cells reversed mitochondrial fusion (Fig EV2). Taken together, these results show that PKD1 regulates adipocyte function primarily by suppressing AMPK.

PKD1 deletion in adipocytes protects against diet-induced obesity

To understand the physiological consequences of PKD1-mediated regulation of energy dissipation and lipogenesis, we investigated the impact of PKD1 action in adipocytes *in vivo*. Activation, abundance, and expression of PKD1 in adipocytes were induced upon feeding (Fig 4A and B). Moreover, in adipose tissue of mice lacking PKD1 in adipocytes (PKD1adipoΔ/Δ) fed ND we observed decreased AMPK alpha phosphorylation at S485/S491, increased phosphorylation of AMPK alpha subunit at T172 and enhanced phosphorylation of AMPK downstream target ACC at S79 (Fig EV3A), suggesting that PKD1 suppresses AMPK activity also in the *in vivo* settings. AMPK is a master activator of autophagy (Kim, Kundu et al., 2011). Interestingly, we observed increased LC3 cleavage in adipose tissue of PKD1adipoΔ/Δ mice fed ND (Fig EV3A) suggesting enhanced autophagy.

Next, we subjected PKD1adipoΔ/Δ and control animals for fasting/refeeding experiment. The total TG, free fatty acids (FFA), glycerol, and glucose levels did not differ from PKD1adipoΔ/Δ compare to control animals at fasted and fasted-refed stage (Fig EV3B-E). Also, the levels of phosphorylation of AMPK alpha subunits at S485/S491 and on T172 as well as phosphorylation of ACC at S79 was not altered by PKD1 deletion during fasting (Fig S4A). However, in adipose tissue of refed animals, deletion of PKD1 resulted in decreased phosphorylation of AMPK alpha subunit at S485/S491 and enhanced phosphorylation of AMPK alpha T172 as well as ACC at S79 (Fig S4B). Altogether, these findings suggest that PKD1 can promote adiposity *in vivo*. To test this hypothesis, we monitored mice lacking PKD1 in adipocytes (PKD1adipoΔ/Δ) for 24 weeks on ND and on HFD. PKD1adipoΔ/Δ mice showed significantly less weight gain when challenged with HFD, whereas no differences could be observed when PKD1adipoΔ/Δ mice were fed ND (Fig 4C). Body composition analysis revealed markedly smaller fat tissue depots as well as reduced liver weight, while weight of other organs was not altered (Fig 4D). Of note,

mice with PKD1 deletion had less gonadal white adipose tissue (gWAT) weight even under ND feeding (Fig S4C). Consistently with our previous findings, we observed increased phosphorylation of ACC at S79 as well as reduced phosphorylation at S485/S491 of AMPK alpha in sWAT isolated from PKD1adipoΔ/Δ fed HFD (Fig EV4A). However, phosphorylation of AMPK alpha at T172 in sWAT of mice fed with HFD for 24 weeks was not altered (Fig EV4A). Interestingly, phosphorylation of AMPK alpha on S485/S49, T172 and ACC at S79 in BAT isolated from HFD and ND fed PKD1adipoΔ/Δ was not changed (Fig EV4B). Furthermore, in PKD1-deficient SVC isolated from BAT no changes in phosphorylation of AMPK alpha on S485/S49, T172 and ACC at S79 were observed (Fig S5A). Metabolic analysis of PKD1adipoΔ/Δ mice showed no significant differences in food intake or activity compared to control animals when fed HFD (Fig 4E and F). Importantly, PKD1adipoΔ/Δ mice fed HFD showed an increase in energy expenditure compared to control animals (Fig 4G). Similar effects were observed in PKD1adipoΔ/Δ mice fed ND (Fig S5B), while other metabolic parameters were not changed (Fig S5C and D). Therefore, deletion of PKD1 specifically in adipocytes protects mice from diet-induced obesity by increasing their energy expenditure.

Consistent with these results, PKD1adipoΔ/Δ mice also showed profoundly changed adipose tissue morphology. The overall adipocyte size was smaller in PKD1adipoΔ/Δ mice as compared to control animals when fed HFD (Fig 4H-L). However, no changes were observed in different types of adipose tissue of mice fed ND (Fig S6A-E). Moreover, we did not observe ectopic myofiber formation within subcutaneous adipose tissue depots of PKD1adipoΔ/Δ mice (Fig S6F and G). Induction of energy expenditure by adipocytes requires a reprogramming of expression patterns of these cells. RNA sequencing revealed that sWAT from PKD1adipoΔ/Δ mice showed elevated expression of genes promoting the creatine-driven substrate cycle, which was recently proposed to promote energy expenditure by adipocytes (Kazak et al., 2015) (Fig 5A). Consistently, genes characteristic for beige adipocytes were also elevated (Fig 5B). Gene set enrichment analysis also revealed elevated expression of genes related to beiging of white

adipocytes in sWAT lacking PKD1 (Fig 5A and B). QPCR analysis confirmed increased expression of genes promoting creatine cycle in the absence of PKD1 (Fig 5C). Moreover, PKD1-deficient sWAT displayed elevated expression of genes promoting energy expenditure (Kajimura et al., 2015) including *Adrb3*, *Ucp1*, *Ucp3*, and *Pgc-1α* while expression of the master regulator of adipocyte differentiation *Pparγ* was not altered (Fig 5C). Similarly, expression of the major genes determining lipid metabolism in adipocytes (*Fasn*, *Dgat*, *Lpl*, *Acc*, *Srebp1*, *Srebp2*, *Creb*, and *Chrebp*) was not altered by PKD1 deletion (Fig S7A). Of note, mitochondrial content in sWAT was markedly elevated in the absence of PKD1 (Fig 5D). Although we did not observe a clear correlation between PKD1 deletion and appearance of multilocular adipocytes (Fig 4H and K), the protein level of the major beige adipocyte marker UCP1, was markedly elevated in PKD1-deficient sWAT (Fig 5E). However, in BAT, expression of these genes was not enhanced upon deletion of PKD1 (Fig S7B). Acquisition of beige adipocyte is largely inhibited at the thermoneutral environment. Importantly, maintenance of PKD1adipoΔ/Δ mice at 30° Celsius resulted in normalization of elevated energy expenditure and reduction of body weight in PKD1 deficient mice (Fig S7C and D). Altogether, these data suggest that deficiency of PKD1 induces beiging in white adipocytes. This elevates whole body energy dissipation and protects PKD1adipoΔ/Δ mice from diet-induced obesity.

PKD1 suppresses ADRB3 expression in an AMPK – C/EBP-α/C/EBP-δ – dependent manner

Next, we tested if the expression of beige/brown markers is altered in isolated adipocytes. The expression of the creatin kinase cycle related genes and selected muscle markers (*Ckm*, *Ckmt2*, *Myh1*, *Myh2*, *Mck*, and *Myg*) was enhanced in differentiated SVC deficient for PKD1 (Fig 6A). However, the expression of *Ucp1* and other classical beige/brown markers (*Ucp3*, *Cidea*, *Cideb*, *Prdm16*, *Bmp7*, *Slc27a1*, *Slc27a2*, *Pgc-1α*, *Pparα*, and *Pparγ*) was not altered by PKD1 deletion (Fig 6A). Interestingly, the expression of the gene encoding for β3-adrenergic receptor

(*Adrb3*) was markedly enhanced in cultured adipocytes lacking PKD1 (Fig 6A). Consistently, immunofluorescence staining revealed elevated levels of β3-adrenergic ADRB3 on the surface of PKD1-deficent adipocytes (Fig 6B). β-adrenergic stimulation results in induction of Ucp1 expression in adipocytes (Kajimura et al., 2015). In fact, stimulation of PKD1-deficient adipocytes and control cells with a β-agonist resulted in enhanced expression of *Ucp1* in the absence of PKD1 (Fig 6C). Altogether, these findings suggest that UCP1 expression in adipose tissue is regulated by PKD1 in an ADRB3-dependent manner. However, the transcription factor mediating PKD1-dependent ADRB3 expression remains unknown. A number of transcription factors mediate beige adipocyte function (Inagaki, Sakai et al., 2016). We measured protein abundance and/or phosphorylation of CtBP1/CtBP2, PGC-1α, C/EBP-α, C/EBP-δ, Rb, FoxO1, C/EBP-β, ERRα, ATF2, CREB, and PRDM16 in 3T3L1 adipocytes expressing PKD1ca (Fig EV5A). Interestingly, expression of PKD1ca resulted in decreased abundance of C/EBP-α and C/EBP-δ (Fig EV5A). Conversely, depletion of adipocytes from PKD1 resulted in elevation of C/EBP-α and C/EBP-δ levels (Fig 6D and E), whereas mRNA levels of both transcription factors remained unchanged (Fig EV5B and C). Of note, stimulation of PKD1ca expressing adipocytes with AICAR resulted in increased C/EBP-α and C/EBP-δ levels in both, control and PKD1ca cells (Fig 6F). Previous studies showed that C/EBP-α and possibly C/EBP-δ are required for ADRB3 expression in adipocytes (Dixon, Daniel et al., 2001). Moreover, deletion of C/EBP-α and C/EBP-δ in mice results in reduction of UCP1 expression in adipose tissue (Tanaka, Yoshida et al., 1997). To test if PKD1 regulates ADRB3 expression in C/EBP-α and/or C/EBP-δ – dependent manner, we silenced these transcription factors in SVC deficient for PKD1. Expression analysis revealed that silencing of both *C/ebp-α* and *C/ebp-δ* (Fig EV5B and C) is sufficient to normalize elevated expression of ADRB3 in cells lacking PKD1 (Fig 6G). Altogether, our data suggest that PKD1 suppresses C/EBP-α and C/EBP-δ abundance in an AMPK-dependent manner and both of these transcription factors promote ADRB3 expression which is required for full induction of beige/brown gene expression.

PKD1 deletion in adipocytes protects against diet-induced fatty liver disease and type 2 diabetes

AMPK protects against fatty liver disease and insulin resistance and its activation can control adipokine levels in the blood (Mottillo, Desjardins et al., 2016, Zhu, Ghoshal et al., 2016). Therefore, we tested these conditions in mice with specific PKD1-deletion in adipocytes.

Levels of adiponectin and resistin in the blood of PKD1adipoΔ/Δ mice were not altered as compared to control animals when fed ND or HFD (Fig S8A and B). However, leptin levels were reduced in PKD1adipoΔ/Δ mice when fed ND, whereas on HDF reduction of leptin levels did not reach significance (P=0.18), most probably due to the high variations induced upon HFD feeding (Fig S8C). Consistently with the fact that PKD1adipoΔ/Δ mice presented decreased adipose tissue content, we also observed that circulating FFA levels were markedly lower in HFD fed mice lacking PKD1 in adipocytes compared to control animals. PKD1adipoΔ/Δ mice fed ND showed moderately reduced FFA levels in the circulation (P=0.13) (Fig 7A). Importantly, levels of another lipolysis product, glycerol, and TG levels were not altered in PKD1adipoΔ/Δ mice (Fig S8D and E). Next, we tested whether PKD1adipoΔ/Δ mice respond better to insulin as predicted by lower FFA levels. Indeed, HFD fed PKD1adipoΔ/Δ mice challenged with insulin injection displayed lower levels of glucose as compared to control animals at all time points tested. PKD1adipoΔ/Δ mice fed ND also showed a moderate but significant improvement of insulin action (Fig 7B). In line with these results, PKD1adipoΔ/Δ mice fed with HFD for 24 weeks displayed improved glucose tolerance, whereas no impact of PKD1 deletion was observed in mice fed ND (Fig 7C). Interestingly, no impact of PKD1 deletion on glucose tolerance has been observed in mice fed HFD for a short period (8 weeks) (Fig S8F), indicating that improved glucose tolerance in mice fed HFD for 24 weeks is secondary to the decreased adiposity. Importantly, improved glucose tolerance in PKD1adipoΔ/Δ mice was specifically caused by a better peripheral insulin sensitivity, since insulin levels were not altered in the absence of PKD1 (Fig S8G). Consistently, activation of

Akt kinase, a key signaling molecule in the insulin pathway, was markedly enhanced in PKD1-deficient adipocytes and reduced in adipocytes with elevated PKD1-dependent signaling (Fig 7D and E).

Obesity is often associated with fatty liver disease. Indeed, we observed a reduced liver weight in PKD1adipoΔ/Δ mice fed HFD (Fig 4D), which could be explained by a reduced triglyceride content in this organ (Fig 7F and G).

To test if PKD1 also regulates insulin sensitivity in humans, we measured expression of PKD1 in sWAT of insulin resistant and control patients. PKD1 levels correlated positively with HOMA-IR (the major parameter for insulin resistance), indicating that PKD1 might regulate insulin sensitivity in human tissues (Fig 7H). Moreover, human adipocytes treated with a PKD-inhibitor presented reduced lipogenesis rate (Fig 7I). Consistently with our previous findings inhibition of PKD in human adipocytes also resulted in higher oxygen consumption at the basal conditions and after oligomycin stimulation (oxygen consumption caused by the decoupling activity) (Fig 7J). Altogether, deletion of PKD1 specifically in adipocytes protects from diet-induced T2D and lipid accumulation in liver. Moreover, the proposed cellular mechanisms of PKD1 action also seems to be valid in human adipocytes.

Next, we tested if abrogation of PKD1-dependent signaling in adipose tissue of mice with established obesity can attenuate the course of this disease. For that purpose we generated mice in which adipocyte specific deletion of PKD1 was induced by tamoxifen administration after 10 weeks of HFD feeding (Fig S8H). Of note, upon deletion of PKD1, mice did not further gain body weight compared to corresponding control animals (Fig 8A). Similarly, the gain of fat mass was almost completely abrogated upon PKD1 deletion while control animals kept accumulating fat (Fig 8B). Consistently with our previous data, PKD1 deletion resulted in a higher energy expenditure without affecting activity and food intake of these mice (Fig 8C-E). Finally, deletion of PKD1 in adipocytes of obese mice resulted in improved glucose tolerance (Fig 8F).

In conclusion, our results demonstrate that deletion of PKD1 promotes beiging in white adipocytes in an AMPK-dependent manner. This results in an elevated whole body energy expenditure and is protective against diet-induced obesity, development of T2D as well as liver steatosis. Therefore, PKD1 could be a new therapeutic target to treat obesity.

Discussion

PKD1-mediated signaling emerges as a master regulator of nutrient and energy homeostasis in health and disease (Bergeron, Ghislain et al., 2017, Goginashvili et al., 2015, Sumara et al., 2009). PKD1 is activated by DAG as well as PKCs (Rozengurt, 2011) and our data suggest that the levels and activity of PKD1 are induced in adipose tissue upon feeding. Moreover, we showed that in adipocytes PKD1 is activated specifically by extracellular purines. However, specific purinergic receptors responsible for PKD1 activation need to be identified. Adipocytes play a central role in the regulation of metabolic homeostasis. Excessive lipid accumulation in white adipocytes is a hallmark of obesity and promotes obesity-related disorders. Importantly, formation of metabolically active beige adipocytes within the white adipose tissue protects against obesity (Kajimura et al., 2015, Kazak et al., 2015). Up to now, the physiological role of PKD1 in adipose tissue and its role in the relevant human diseases remained unknown. Here, we showed that PKD1 expressed in adipocytes plays a crucial role in the whole body energy homeostasis. PKD1adipoΔ/Δ mice are resistant to diet-induced obesity. They display higher energy expenditure, lower content of adipose tissue, and smaller adipocytes. Moreover, sWAT depots contained higher numbers of mitochondria and showed increased expression of genes responsible for energy dissipation. Interestingly, we observed elevated expression of classical genes involved in adaptive thermogenesis (e.g. *Adrb3*, *Ucp1*, *Pgc-1α* and *Ucp3*) and genes promoting creatine-driven substrate cycle (*Ckm*, *Ckmt2*), suggesting that PKD1 can suppress energy dissipation by adipocytes using several complementary mechanisms. Although, we did not observe a clear correlation between the absence of PKD1 and appearance of multilocular cells within subcutaneous depot of adipose tissue, the protein abundance of UCP1 was clearly elevated in the absence of PKD1. Of note, in several other mouse models, increased UCP1 abundance was observed in unilocular adipocytes (Rossmeisl, Barbatelli et al., 2002, Schneider, Valdez et al., 2016, Zheng, Lin et al., 2017). However, in the isolated PKD1-deficient adipocytes we observed elevated gene expression of *Adrb3* but *Ucp1* levels were not altered at

basal conditions. In fact, our data suggest that induction of UCP1 expression by PKD1 deletion requires presence of the ligand for β3-adrenergic receptor, as addition of β-agonists to the media of cultured adipocytes resulted in increased expression of UCP1 in the absence of PKD1. Furthermore, our data suggests that PKD1 regulates ADRB3 expression by targeting C/EBP-α and C/EBP-δ in an AMPK-dependent manner. Of note, we did not observe enhanced expression of thermogenic genes in BAT of PKD1adipoΔ/Δ mice. Moreover, AMPK-dependent signaling does not seem to be affected by the deletion of PKD1 in BAT. This result is in agreement with the fact that the deletion of PKD1 in isolated brown adipocytes did not affect basal respiration and energy dissipation. Taken together, our data indicate that PKD1 deletion promotes beiging in WAT, but does not affect brown adipocytes.

In addition, our data suggest an alternative way to support uncoupling respiration in adipocytes by regulating mitochondrial dynamics. A previous study revealed that β-adrenergic stimulation increases mitochondrial fission in brown adipocytes leading to thermogenic activation and increased oxygen consumption (Wikstrom et al., 2014). Moreover, ablation of PPARγ target Bnip3 promotes mitochondrial fusion in white adipocytes, which results in suppression of energy dissipation (Tol et al., 2016). Our results indicate that the deletion of PKD1 increases mitochondrial fragmentation, which positively correlates with higher energy dissipation in adipocytes. Therefore, PKD1 represents the first identified signaling module (kinase) suppressing mitochondrial fragmentation to decrease energy dissipation by adipocytes.

Importantly, our data link PKD1 signaling to the key regulator of adipocyte function, AMPK. A recent study indicates that PKD1 suppresses activity of AMPK by phosphorylation of its alpha subunit in muscle cells *in vitro* (Coughlan et al., 2016). Our results show that PKD1 suppresses AMPK activity also in adipocytes. Of note, we showed that deletion of PKD1 in mice results in an enhanced AMPK signaling in subcutaneous depots of adipose tissue derived from mice fed ND or HFD. However, unlike other markers of AMPK activation, phosphorylation of T172 of AMPK alpha subunit in adipose tissue of mice fed HFD for 24

weeks was not clearly enhanced by PKD1 deletion. This indicates that prolonged HFD feeding might induce additional signaling cascades which partially mask the effect of PKD1 deletion. AMPK promotes mitochondrial biogenesis as well as the expression of genes involved in energy dissipation by adipocytes and suppresses lipogenesis (Bijland et al., 2013, Mottillo et al., 2016, Zhu et al., 2016). Consistently, PKD1 drives lipogenesis, reduces mitochondrial content and lowers energy dissipation by adipose tissue. AMPK suppresses lipogenesis by phosphorylating and inhibiting the action of ACC (Bijland et al., 2013). Consistently, the ACC phosphorylation of S79 was elevated in the absence of PKD1, but the expression of genes implicated in lipid synthesis was not altered. AMPK activation in multiple cell lines lead to the induction of autophagy in a mTORC1-dependent and independent manner (Roach, 2011). In line with these data, we observed that PKD1 deletion leads to elevation of autophagy marker - LC3 cleavage. Induction of autophagy promotes beige to white adipocyte transition (Altshuler-Keylin, Shinoda et al., 2016). Moreover, ATG7 deletion, which is required for induction of autophagy, results in a beiging-like phenotype (Singh, Xiang et al., 2009, Zhang, Goldman et al., 2009). However, the activation of AMPK in adipocytes promotes energy expenditure and protects against obesity (Gaidhu, Frontini et al., 2011, Zhang, Zhang et al., 2014, Zhu et al., 2016). Therefore, our data support the notion that AMPK promote energy dissipation by adipocytes by utilizing autophagy-independent mechanisms. Additionally, in other cell types AMPK promotes mitochondrial fragmentation (Toyama, Herzig et al., 2016), while our results indicate that PKD1 suppresses this process. Moreover, the effect of overexpression of PKD1ca on mitochondrial aggregation are fully reversible by manipulation of AMPK activity. A number of studies aimed to define the AMPK impact on the regulation of lipolysis. Both, anti- and pro-lipolytic effects of AMPK have been reported (Bijland et al., 2013, Djouder, Tuerk et al., 2010). A recent genetic study revealed that ablation of AMPK activity in adipocytes does not affect β-adrenergic-induced lipolysis in mice (Mottillo et al., 2016). However, during cancer-associated cachexia loss of AMPK activity promotes both lipolysis and lipogenesis, which results in

energy dissipation by adipocytes (Rohm, Schafer et al., 2016). Our results indicate that PKD1 does not affect basal and β-adrenergic-induced lipolysis in isolated adipocytes. Also the levels of FFAs and glycerol of fasted young-adult (8 weeks old) PKD1-deficient mice are not altered. However, we showed that FFA levels are reduced in mice lacking PKD1, which is probably caused by the decreased adipose tissue content. Similarly to the deletion of PKD1, elevation of AMPK signaling in adipocytes by genetic manipulations or pharmacological interventions ameliorates diet-induced obesity, insulin resistance and hepatic steatosis by enhancing energy expenditure of animals (Gaidhu et al., 2011, Zhang et al., 2014, Zhu et al., 2016).

Expression of PKD1 in adipocytes promotes insulin resistance and mice lacking PKD1 present improved insulin sensitivity, glucose tolerance, and protection against liver steatosis. However, PKD1 in cardiomyocytes rather promotes insulin sensitivity (Dirkx, van Eys et al., 2014), indicating that the impact of PKD1 on insulin signaling might depend on the cellular context. Alternatively, improved insulin sensitivity in the absence of PKD1 in adipocytes might be secondary to the reduced lipid accumulation. Strikingly, however, we demonstrated that PKD1 expression in human adipose tissue correlates with insulin sensitivity. Moreover, in line with our data obtained in rodents, we showed that inhibition of PKD in human adipocytes promotes energy dissipation and suppresses lipogenesis, which indicates the presented mechanisms are conserved in humans.

Taken together, our data provide evidence for the crucial role of PKD1 signaling in fat tissue and energy homeostasis *in vivo*. We predict that inhibition of PKD1 specifically in fat tissue represents an attractive strategy for the development of precision medicine to treat obesity and diabetes in the future.

Materials and Methods

Pre-adipocyte culture and differentiation

3T3L1 pre-adipocytes (ATCC) were cultured in Dulbecco's modified eagle's medium (DMEM), 10% fetal calf serum (FCS), and 40µg/mL gentamycin and differentiated into adipocytes as previously described (Cai, El-Merahbi et al., 2017). T37I cells were cultured in DMEM-F12, 10% FCS, and 1% sodium pyruvate (SP). Differentiation was induced 2 days post-confluence by adding 2nM T3-hormone and 1,5 µg/ml insulin for 7 days to achieve full differentiation as described before (Zennaro, Le Menuet et al., 1998). Stromal vascular cells (SVC) from subcutaneous white adipose tissue (sWAT) and brown adipose tissue (BAT) of 5-9 weeks old mice were isolated and differentiated into mature adipocytes. Concisely, sWAT or BAT was collected from mice, minced, and treated with 2mg/mL collagenase D (11088882001, Roche) in PBS containing 5mM $CaCl_2$ and 1% BSA for 40minutes. After hemolysis and filtration of adipose tissue through a 40 µm mesh, the sample was washed in PBS by centrifugation and cultured in DMEM/F-12 containing 10% FBS, 1% SP, 1% non-essential amino acids (NEAA) and 1% Penicillin-Streptomycin (P/S). Two days post-confluence, SVC differentiation was induced by adding a cocktail including 0.2 µM indomethacin, 1 µM dexamethasone, 0.5 mM IBMX and 1.5 µg/ml insulin for the first 4 days, followed by insulin treatment for additional 4 days to achieve differentiation into adipocytes. In SVC derived from BAT, additionally 100 nM T3 2 nM was added to the medium throughout differentiation. Before treatment, cells were serum starved for 2 hours in DMEM supplemented with 0.5% BSA and afterwards stimulated with 100 nM insulin for 10 minutes. In addition, in certain experiment 2 mM AICAR (Sigma) was added to the medium for 2 hours. In case of PKD1 stimulation assessment, cells were serum starved for 2 hours followed by 100 µM 1,2-dioctanoyl-sn-glycerol (DAG) (Enzo Life Science) stimulation for 2 or 4 hours or stimulation with Insulin (Sigma) (10 nM / 100nM), Carbachol (Tocris) (1 µM / 10 µM), Isoproterenol (Sigma) (1 µM / 10 µM), Serotonin (Sigma) (50 µM / 250 µM), ATP (Sigma) (10 mM / 300 mM), and ADP

(Sigma) (100 mM / 300 mM). Afterwards, cell lysates were used for Western blot analysis. In case of lipogenesis assay, cells were serum starved for 3 hours. SVC isolated from sWAT were serum starved for 2 hours followed by 24 hours stimulation with Isoproterenol (0.1 μM, 1 μM, and 10 μM) for further qPCR analysis. Human subcutaneous preadipocytes (ATCC) were cultured and differentiated into adipocytes according to the manufacturer's protocol. Differentiated human preadipocytes were pretreated with 3 μM CRT 0066101 (Tocris) for 3 days and used to measure lipogenesis rate or mitochondrial fragmentation.

Explants derived from sWAT

Explants from freshly harvested mouse subcutaneous adipose tissue (sWAT) were removed from the mouse. After removal of fibrotic tissue and obvious vasculature, the tissue was cut into roughly 15 mg of tissue pieces, which were embedded in the individual tubes filled with DMEM and 0.5% BSA for 2 hours at 37°C to equilibrate. Explants were either used for WB analysis afterwards or lipogenesis assay was performed in these explants with additional Compound C (CC) (Tocris) (5 μM) treatment for 4 hours.

PKD1 flox/flox Adiponectin Cre mice (PKD1adipo Δ/Δ) and tamoxifen-inducible strain (PKD1ind.adipo Δ/Δ)

All animal studies were approved by the local institutional animal care (Regierung von Unterfranken, Germany) and conducted according to the guidelines and state regulations. Animal protocol number AK 55.2-2531.01-124/13, approved on 28.01.2014. $PKD1^{flox/flox}$ mice (Fielitz et al., 2008) were cross-bred with adiponectin promoter–driven Cre mice (Eguchi et al., 2011) (Jackson Laboratory) or adiponectin promoter-driven Cre-ERT mice (Sassmann, Offermanns et al., 2010) (Jackson Laboratory), which resulted in mice with targeted deletion of PKD1 in adipocytes of white and brown adipose tissue from the beginning or after induction with 100 mg/kg Tamoxifen injection for 5 consecutive days. Genotyping protocols for the given mouse lines are available from Jackson Laboratory. Mice were kept in cages from Tecniplast

(#GM500PFS) in a green Line IVC-rack system and provided with sterile water and irradiated rodent normal diet (sniff Spezialdiäten) at all times, which was only removed or exchanged if necessary for an experiment. High fat diet (HFD) (ResearchDiets) was given to mice when indicated. In case of thermoneutral conditions, mice were kept at 30°C during the experiment.

Human samples

The human studies were approved by the Ethics Committee of the University Hospital of Salamanca and all subjects provided written informed consent to undergo subcutaneous fat biopsy under direct vision during surgery. The study population included adults who underwent elective bariatric surgery at the University Hospital of Salamanca. Patients were excluded if they had a history of alcohol abuse or excessive alcohol consumption (>30 g/day in men and > 20 g/day in women), or chronic hepatitis C or B or diabetes. Data were collected on demographic information (age, sex, and ethnicity), anthropomorphic measurements (BMI), smoking and alcohol history, coexisting medical conditions, and medication use. Fasting venous blood samples were collected and sWAT was obtained during surgery and frozen for posterior analysis.

AMP activity assay

To measure AMPK activity in cell lysates the immunoassay CycLex AMPK Kinase Assay Kit (MBL International Corporation) was used. For CycLex AMPK Kinase Assay, differentiated 3T3L1 cells were serum starved for 2 hours followed by 100 nM Insulin stimulation for 10 minutes. Cell lysates were collected and AMPK activity was measured following the manufacturer's instructions. Absorbance was read at 450 nm/ 540 nm with (Zennaro et al., 1998)Spark 10M microplate reader (Tecan). Results were normalized to protein content, after background subtraction.

Quantification of triglyceride accumulation and lipolysis rate

The amount of triglycerides normalized to DNA content of the cells was assessed by double staining of AdipoRed reagent (Lonza) and Hoechst 33342 (Thermo Fischer Scientific) according to manufacturers' protocols. Oil-Red O staining was used to visualize the multiple intracellular lipid droplets in cells. Briefly, once fully differentiated, cells were fixed with 10% formaldehyde for 30 minutes and Oil Red O solution was added for 1 hour. For certain experiments, cells were either transfected with siRNA against AMPKα1/α2 subunits for 48 hours or pretreated with 0.5 mM AICAR for 3 days. To assess lipolysis rate, cells were serum starved for 2 hours in phenol red-free DMEM supplemented with 0.5% BSA and afterwards stimulated with 10 μM isoproterenol (Iso) (Sigma-Aldrich) for 2 hours in the fresh medium. FFAs in the medium were measured using NEFA-reagents (Wako) and glycerol was quantified by free glycerol reagent (Sigma-Aldrich) according to the manufacturers' instructions.

Lipogenesis Assay

Cells were incubated in 1 μCi/mL D-[3-^{3}H]-glucose (Perkin Elmer) for 3 hours in the presence or absence of 100 nM insulin. Total intracellular lipids were extracted with a mixture of chloroform and methanol (2:1, v/v). After centrifugation, chloroform phase was transferred into a scintillation vial and 4mL of scintillation liquid was added before counting. De novo lipogenesis rates were normalized to protein levels using Quick Start Bradford Protein Assay (Bio-Rad). For certain experiments, cells were either transfected with siRNA against AMPKα1/α2 subunits for 48 hours or pretreated with 2 mM AICAR for 2 hours.

Mitochondrial respiration

Mitochondrial respiration was determined by measuring oxygen consumption rate (OCR) using the Seahorse XF Cell Mito Stress Test (103015-100; Agilent Technologies) in a Seahorse XFe96 Analyzer according to the manufacturer's protocol. Briefly, cells were incubated for 1 hour with 175 μl Seahorse assay medium containing 1 mM sodium pyruvate, 2 mM glutamine and 5 mM glucose. Meanwhile, the Seahorse sensor cartridge ports were loaded with 25 μl of

inhibitors to have a final concentration of 2 μM oligomycin (port A), 1 μM FCCP (port B) and 0.75 μM rotenone/antimycin A (port C). The experimental design was setup using the WAVE software program and measurement was performed in the Seahorse XFe96 Analyzer. Normalization to the DNA content was conducted by fixing the cells in 75% ethanol, followed by staining with Crystal Violet (Sigma-Aldrich) for 30 minutes, washed with water and air-dried. Afterwards, Crystal Violet was dissolved in 10% acidic acid and the absorption was measured at 590 nm in a Spark 10 M microplate reader (Tecan). For certain experiments, cells were either transfected with siRNA against AMPKα1/α2 subunits for 48 hours or pretreated with 0.5 mM AICAR for 3 days.

Western blot

Western blot analysis was performed according to standard procedures, by running the proteins on an 8%-10% SDS-PAGE, transferring it onto polyvinylidene fluoride (PVDF) membranes (Millipore), and then probing the membrane with primary antibodies against: AMPKα (D5A2) Rabbit mAb (Cell Signaling Technology #5831), Phospho-AMPKα1 (Ser485) /AMPKα2 (Ser491) Rabbit Ab (Cell Signaling Technology #4185), Phospho-AMPKα (Thr172) (40H9) Rabbit mAb (Cell Signaling Technology #2535), Acetyl-CoA Carboxylase (C83B10) Rabbit mAb (Cell Signaling Technology #3676), Phospho-Acetyl-CoA Carboxylase (Ser79) (D7D11) Rabbit mAb (Cell Signaling Technology #11818), PKD/PKCμ Rabbit Ab (Cell Signaling Technology #2052), Phospho-PKD/PKCμ (Ser916) Rabbit Ab (Cell Signaling Technology #2051), Phospho PKD/PKCμ (Ser744/748) Rabbit Ab (Cell Signaling Technology #2054), β-Actin Mouse mAb (Sigma-Aldrich #A5441), GAPDH Rabbit Ab (Sigma-Aldrich #G9545), α-Tubulin Rabbit Ab (Cell Signaling Technology #2144), Phospho-Akt (Ser473) Rabbit Ab (Cell Signaling Technology #9271), Myc-Tag (9B11) Mouse mAb (Cell Signaling Technology #2276), PPARγ (81B8) Rabbit mAb (Cell Signaling Technology #2443), HSL Rabbit Ab (Cell Signaling Technology #4107), ATGL (30A4) Rabbit mAb (Cell Signaling Technology #2439),

or Perilipin (D1D8) Rabbit mAb (Cell Signaling Technology #9349), Anti-UCP1 antibody (Abcam #ab10983), Phospho-CtBP1/CtBP2 (Ser158, Ser164) Polyclonal Antibody (Thermo Fischer Scientific #PA5-64665), PGC-1α (3G6) Rabbit mAb (Cell Signaling Technology #2178), C/EBPα (D56F10) Rabbit mAb (Cell Signaling Technology #8178), C/EBPδ Rabbit Ab (Cell Signaling Technology #2318), Phospho-Rb (Ser807/811) (D20B12) Rabbit mAb (Cell Signaling Technology #8516), Phospho-FoxO1 (Ser256) Ab (Cell Signaling Technology #9461), C/EBPβ (LAP) Ab (Cell Signaling Technology #3087), ERRα (E1G1J) Rabbit mAb (Cell Signaling Technology #13826), Phospho-ATF-2 (Thr71) (11G2) Rabbit mAb (Cell Signaling Technology #5112), Phospho-CREB (Ser133) (87G3) Rabbit mAb (Cell Signaling Technology #9198), Phospho-C/EBPβ (Thr235) Ab (Cell Signaling Technology #3084), Anti-PRDM16 antibody (Abcam #ab106410). After incubation with corresponding horseradish peroxidase (HRP)-conjugated secondary antibodies, proteins were visualized by ECL (Bio-Rad) using X-ray films.

Real Time PCR analysis

Total RNA was extracted from cells and tissue pieces according to the QIAzol Handbook using the RNeasy Plus Universal Tissue Mini Kit (Qiagen). RNA concentration was spectophotometrically (Nanodrop, Thermo Fischer Scientific) determined and first strand cDNA was synthesized by First Strand cDNA Synthesis Kit (Thermo Fischer Scientific) according to the manufacturer's protocol. Real time quantitative polymerase chain reaction (RT-qPCR) was performed using SYBR green Universal PCR master mix (Thermo Fischer Scientific) on a QuantStudio 5 Real Time PCR System (Thermo Fischer Scientific). Expression of all genes was normalized to the *Rpl13a* housekeeping gene (Appendix Table S1). Mitochondrial DNA (mtDNA) copy number was analyzed from total DNA isolated from differentiated SVC as well as snap frozen sWAT samples, according to the manufacturer's instructions using the DNeasy Blood & Tissue Kit (Qiagen). mtDNA was normalized to genomic DNA (gDNA) (Appendix Table S1) by RT-qPCR. For analysis of PKD1 expression

in humans, sWAT was obtained during surgery and frozen to posterior analysis. From this tissue, 1 mg of RNA was extracted with RNeasy Plus Mini kit (Qiagen) following manufacturer's instructions, and further transcribed to cDNA. RT-PCR was performed using Fast TaqMan probe (Thermo Fischer Scientific) and the appropriate TaqMan Assay (Thermo Fischer Scientific) in the 7900 Fast Real Time thermocycler. Relative mRNA expression was normalized to *18s* mRNA measured in each sample.

Mitochondrial staining

For analysis of mitochondrial morphology, cells were plated on a cover slider overnight. Mitochondria were stained by adding 150 nM MitoTracker Red (Thermo Fischer Scientific) in the suitable growth medium for 30 minutes at 37°C. The cells were fixed with 4% PFA for 20 minutes. After washing with PBS 1x, cells were permeabilized by adding ice cold methanol for 5 minutes. Cover slides were mounted using ProLong Gold Antifade Mountant with DAPI (Thermo Fischer Scientific). In case of AICAR treatment, 2 mM AICAR were added 2 hours prior to the fixation. Cells were imaged using a fluorescent microscope (Leica). To quantify mitochondrial morphology in stained differentiated adipocytes, grouping into the different categories was done blindly to genotype and treatment. Cells were defined as fragmented (fragm.) when mitochondria were spherical with no clear length or width. When mitochondria were highly interconnected and elongated, the cells were clustered as fused. All the cells in between were counted as intermediate (interm.).

Immunofluorescent staining of Adrb3

Cells were fixed in 4% PFA and stained according to the standard procedure. Primary antibody against ADRB3 (Anti-beta 3-adrenergic Receptor antibody – Abcam #ab59685) and were used. ProLong Gold Antifade Mountant with DAPI (Thermo Fischer Scientific) was used for mounting. Cells were imaged using a fluorescent microscope (Leica). Fluorescent intensity of the single cells (about 120 cells per genotype) was quantified using Image J software.

RNA sequencing

RNeasy mini columns (Qiagen) with on-column DNase I digestion were used to extract total RNA from tissue samples. PolyA+-RNA was extracted from total RNA using the NEBNext® Poly(A) mRNA Magnetic Isolation Module (NEB). Preparation of sequencing libraries was performed using the NEBNext® Ultra™ RNA Library Prep Kit for Illumina (NEB) including the use of Agencourt AMPure XP Beads (Beckman Coulter) for size-selection and purification of the libraries. The Experion Automated Electrophoresis System (Bio-Rad) was used for library quantification and quality control. All samples were sequenced on a NextSeq500 System (Illumina) and base calling was done with Illumina's FASTQ Generation software v1.0.0. The FastQC script (Babraham Bioinformatics) was used to determine overall sequencing quality. Fastq files were mapped to mm9 using Bowtie2 with default settings and the countOverlaps function from the R package GenomicRanges was used to count reads per gene. Following removal of weakly expressed genes (mean CPM over all samples <1), the differential expression of the remaining genes was called using EdgeR. GSE analyses (Subramanian, Tamayo et al., 2005) were done using signal2noise metric, 1000 permutations and the C2 gene set collection (v6.0) of MSigDB. In some cases, the C2 gene set collection was spiked with a gene signature of published markers for browning.

Histological analysis

For histological analysis, adipose tissues were fixed in 10% formaldehyde and embedded in paraffin. The sections (4-5µm) were stained with hematoxylin-eosin (H&E) according to the standard procedure. Livers were embedded in OCT-Tissue-Tek (SAKURA FINETEK USA INC) and frozen sections were stained according to the standard procedure. Briefly, frozen liver sections (5µm) were stained in a 0.375% Oil Red O solution (3:2 isopropanol:ddH2O, v/v) for 10min. Subsequently, the sections were rinsed under running tap water for 30 min and embedded in a water-soluble mounting medium. For immunohistochemistry, primary antibody

to heavy chain Myosin (Abcam #124205) was used after rehydration and epitope retrieval and later detected with SignalStain® (Cell Signaling) according to the standard procedure. Quadriceps sections were used as positive controls.

Cell size quantification

Images from H&E stained sections of gonadal white adipose tissue (gWAT) and sWAT from mice under normal or high-fat diet were taken with 20x magnification under the microscope. 4 representative pictures were analyzed from each sample by manually measuring the area of each cell in a total area of 0.6mm^2. ImageJ was utilized for this measurement by using the tool, which allows manually encircling of each cell, and automatic measurement of the area.

Liver triglyceride extraction

Frozen liver pieces were homogenized in PBS and lipids were extracted with a mixture of 2:1 chloroform: methanol (v/v). The lipid-containing chloroform phase was dried under nitrogen flow and lipids were re-solubilized in 15 % Triton X-100. Liver triglycerides were quantified using the commercial glycerol and triglyceride reagents according to manufacturer's instructions and normalized to total protein amount.

Glucose and insulin tolerance tests

Glucose tolerance test (GTT) was performed in 4 hours fasted mice at week 8 and 18 of high fat diet (HFD) and week 18 of normal diet (ND). Insulin tolerance test (ITT) after 20 weeks of ND or HFD feeding. A defined dose of glucose (Roth) (1g/kg BW) or insulin (Sanofi-Aventis) (0.25U/kg BW) were injected and glucose removal from the blood was measured prior to the test, 15, 30, 60, 90 and 120 minutes after intraperitoneal injection. Blood glucose levels were assessed from tail vein blood by an automated glucometer (Accu-Chek, Roche).

Indirect calorimetry analysis

Body weight gain of mice was monitored every other week and food intake, energy expenditure and voluntary movements were measured at the end of respective diets using the Phenomaster system (TSE) in mice housed at 23° or 30°Celsius as described before (Trujillo Viera, El-Merahbi et al., 2016).

Analysis of blood samples in mice and humans

FFAs, glycerol and triglycerides were determined from serum of mice using NEFA (Lonza), free glycerol and triglyceride reagents (both Sigma-Aldrich) according to the manufacturers' instructions. Analysis of adiponectin, leptin, resistin and insulin were performed by a magnetic-bead based multiplex Elisa assay (Bio-Rad) on a MagPix Systems (Bio-Rad) according to the manufacturer's guidelines. We collected blood samples for measuring complete cell blood count, as well as glucose using a standard glucometer. Blood samples were also centrifuged, and plasma was frozen to detect insulin by Luminex assay (Appendix Table S2). Individually matched glucose and insulin levels were used to assess HOMA-IR as previously described using the following calculations: HOMA-IR = [glucose (mg/dl) x insulin (mU/l)/405].

Statistical analysis

All data, unless otherwise indicated, are presented as mean values ± standard error of the mean (SEM). Data set comparisons of more than two groups were analyzed using one-way analysis of variance (ANOVA) followed by the Post hoc Tukey test. Determination of significances between two independent groups was determined with unpaired, two-tailed Student's T-Test. P-values at the level of 0.05 were considered statistically significant. Each figure gives exact statistical indications.

Data availability

The RNA-sequencing raw- and processed datasets as well as information on data processing have been deposited in NCBI Gene Expression Omnibus under the accession number: GSE104797.

Acknowledgements

We thank Dr. Olga Sumara, Prof. Dr. Bernhard Nieswandt, and Dr. Izabela Sumara for critical comments to our manuscript. We thank Dr. Marc Lombes for kindly providing us the T37I cells. This project was supported by the Starting Grant (SicMetabol) from the European Research Council (ERC) and internal funds of the Rudolf Virchow Center. Additionally, J. Trujillo, R. El-Merabih and G. Sumara are supported by the Emmy Noether grant from the German Research Foundation (Number Su 820/1-1). The authors declare no conflict of interests and no competing financial interest. G. Sabio received funding from the European Union's Seventh Framework Program (FP7/2007-2013) under grant agreement n° ERC 260464, EFSD/Lilly, MINECO-FEDER SAF2016-79126-R, and Comunidad de Madrid S2010/BMD-2326; to M.M.: ISCIII and FEDER, PI10/01692, and I3SNS-INT12/049.

Author contributions

M. C. L. performed most of the experiments and largely contributed to writing as well as the experimental design. G. S. wrote the manuscript and was responsible for the experimental design. A. E. M., J. T. V., R. E.-M, A. L. V, T. K., W. S., A. S., M. E., S. J.-R., N. M., J. L. T. and M. M. performed part of the experiments. C. P. A. performed high-throughput sequencing and analysis of RNA-sequencing data. G. S., A. S. and M. E. contributed to the experimental design.

Conflict of interest

The authors have declared that no conflict of interest exists.

References

Altshuler-Keylin S, Shinoda K, Hasegawa Y, Ikeda K, Hong H, Kang Q, Yang Y, Perera RM, Debnath J, Kajimura S (2016) Beige adipocyte maintenance is regulated by autophagy-induced mitochondrial clearance. Cell metabolism 24: 402-419

Bergeron V, Ghislain J, Vivot K, Tamarina N, Philipson LH, Fielitz J, Poitout V (2017) Deletion of protein kinase D1 in pancreatic beta cells impairs insulin secretion in high-fat fed mice. Diabetes: db170982

Bergeron V, Ghislain J, Vivot K, Tamarina N, Philipson LH, Fielitz J, Poitout V (2018) Deletion of Protein Kinase D1 in Pancreatic beta-Cells Impairs Insulin Secretion in High-Fat Diet-Fed Mice. Diabetes 67: 71-77

Bijland S, Mancini SJ, Salt IP (2013) Role of AMP-activated protein kinase in adipose tissue metabolism and inflammation. Clin Sci (Lond) 124: 491-507

Cai K, El-Merahbi R, Loeffler M, Mayer AE, Sumara G (2017) Ndrg1 promotes adipocyte differentiation and sustains their function. Sci Rep 7: 7191

Coughlan KA, Valentine RJ, Sudit BS, Allen K, Dagon Y, Kahn BB, Ruderman NB, Saha AK (2016) PKD1 Inhibits AMPKalpha2 through Phosphorylation of Serine 491 and Impairs Insulin Signaling in Skeletal Muscle Cells. J Biol Chem 291: 5664-75

Dirkx E, van Eys GJ, Schwenk RW, Steinbusch LK, Hoebers N, Coumans WA, Peters T, Janssen BJ, Brans B, Vogg AT, Neumann D, Glatz JF, Luiken JJ (2014) Protein kinase-D1 overexpression prevents lipid-induced cardiac insulin resistance. J Mol Cell Cardiol 76: 208-17

Dixon TM, Daniel KW, Farmer SR, Collins S (2001) CCAAT/Enhancer-binding Protein α Is Required for Transcription of the β3-Adrenergic Receptor Gene during Adipogenesis. Journal of Biological Chemistry 276: 722-728

Djouder N, Tuerk RD, Suter M, Salvioni P, Thali RF, Scholz R, Vaahtomeri K, Auchli Y, Rechsteiner H, Brunisholz RA, Viollet B, Makela TP, Wallimann T, Neumann D, Krek W (2010) PKA phosphorylates and inactivates AMPKalpha to promote efficient lipolysis. EMBO J 29: 469-81

Eguchi J, Wang X, Yu S, Kershaw EE, Chiu PC, Dushay J, Estall JL, Klein U, Maratos-Flier E, Rosen ED (2011) Transcriptional control of adipose lipid handling by IRF4. Cell Metab 13: 249-59

El-Merahbi R, Loffler M, Mayer A, Sumara G (2015) The roles of peripheral serotonin in metabolic homeostasis. FEBS Lett 589: 1728-34

Ferdaoussi M, Bergeron V, Zarrouki B, Kolic J, Cantley J, Fielitz J, Olson EN, Prentki M, Biden T, MacDonald PE, Poitout V (2012) G protein-coupled receptor (GPR)40-dependent potentiation of insulin secretion in mouse islets is mediated by protein kinase D1. Diabetologia 55: 2682-2692

Fielitz J, Kim MS, Shelton JM, Qi X, Hill JA, Richardson JA, Bassel-Duby R, Olson EN (2008) Requirement of protein kinase D1 for pathological cardiac remodeling. Proc Natl Acad Sci U S A 105: 3059-63

Gaidhu MP, Frontini A, Hung S, Pistor K, Cinti S, Ceddia RB (2011) Chronic AMP-kinase activation with AICAR reduces adiposity by remodeling adipocyte metabolism and increasing leptin sensitivity. J Lipid Res 52: 1702-11

Gehart H, Goginashvili A, Beck R, Morvan J, Erbs E, Formentini I, De Matteis MA, Schwab Y, Wieland FT, Ricci R (2012) The BAR domain protein Arfaptin-1 controls secretory granule biogenesis at the trans-Golgi network. Dev Cell 23: 756-68

Goginashvili A, Zhang Z, Erbs E, Spiegelhalter C, Kessler P, Mihlan M, Pasquier A, Krupina K, Schieber N, Cinque L, Morvan J, Sumara I, Schwab Y, Settembre C, Ricci R (2015) Insulin granules. Insulin secretory granules control autophagy in pancreatic beta cells. Science 347: 878-82

Inagaki T, Sakai J, Kajimura S (2016) Transcriptional and epigenetic control of brown and beige adipose cell fate and function. Nature reviews Molecular cell biology 17: 480

Ittner A, Block H, Reichel CA, Varjosalo M, Gehart H, Sumara G, Gstaiger M, Krombach F, Zarbock A, Ricci R (2012) Regulation of PTEN activity by p38delta-PKD1 signaling in neutrophils confers inflammatory responses in the lung. J Exp Med 209: 2229-46

Kajimura S, Saito M (2014) A new era in brown adipose tissue biology: molecular control of brown fat development and energy homeostasis. Annu Rev Physiol 76: 225-49

Kajimura S, Spiegelman BM, Seale P (2015) Brown and Beige Fat: Physiological Roles beyond Heat Generation. Cell Metab 22: 546-59

Kazak L, Chouchani ET, Jedrychowski MP, Erickson BK, Shinoda K, Cohen P, Vetrivelan R, Lu GZ, Laznik-Bogoslavski D, Hasenfuss SC, Kajimura S, Gygi SP, Spiegelman BM (2015) A creatine-driven substrate cycle enhances energy expenditure and thermogenesis in beige fat. Cell 163: 643-55
Kim J, Kundu M, Viollet B, Guan K-L (2011) AMPK and mTOR regulate autophagy through direct phosphorylation of Ulk1. Nature cell biology 13: 132
Kim MS, Fielitz J, McAnally J, Shelton JM, Lemon DD, McKinsey TA, Richardson JA, Bassel-Duby R, Olson EN (2008) Protein kinase D1 stimulates MEF2 activity in skeletal muscle and enhances muscle performance. Mol Cell Biol 28: 3600-9
Matthews SA, Liu P, Spitaler M, Olson EN, McKinsey TA, Cantrell DA, Scharenberg AM (2006) Essential role for protein kinase D family kinases in the regulation of class II histone deacetylases in B lymphocytes. Mol Cell Biol 26: 1569-77
Mottillo EP, Desjardins EM, Crane JD, Smith BK, Green AE, Ducommun S, Henriksen TI, Rebalka IA, Razi A, Sakamoto K, Scheele C, Kemp BE, Hawke TJ, Ortega J, Granneman JG, Steinberg GR (2016) Lack of Adipocyte AMPK Exacerbates Insulin Resistance and Hepatic Steatosis through Brown and Beige Adipose Tissue Function. Cell Metab 24: 118-29
Muller TD, Lee SJ, Jastroch M, Kabra D, Stemmer K, Aichler M, Abplanalp B, Ananthakrishnan G, Bhardwaj N, Collins S, Divanovic S, Endele M, Finan B, Gao Y, Habegger KM, Hembree J, Heppner KM, Hofmann S, Holland J, Kuchler D et al. (2013) p62 links beta-adrenergic input to mitochondrial function and thermogenesis. J Clin Invest 123: 469-78
Roach PJ (2011) AMPK→ uLK1→ autophagy. Molecular and cellular biology 31: 3082-3084
Rohm M, Schafer M, Laurent V, Ustunel BE, Niopek K, Algire C, Hautzinger O, Sijmonsma TP, Zota A, Medrikova D, Pellegata NS, Ryden M, Kulyte A, Dahlman I, Arner P, Petrovic N, Cannon B, Amri EZ, Kemp BE, Steinberg GR et al. (2016) An AMP-activated protein kinase-stabilizing peptide ameliorates adipose tissue wasting in cancer cachexia in mice. Nat Med 22: 1120-1130
Rosen ED, Spiegelman BM (2006) Adipocytes as regulators of energy balance and glucose homeostasis. Nature 444: 847-53
Rossmeisl M, Barbatelli G, Flachs P, Brauner P, Zingaretti MC, Marelli M, Janovská P, Horáková M, Syrový I, Cinti S (2002) Expression of the uncoupling protein 1 from the aP2 gene promoter stimulates mitochondrial biogenesis in unilocular adipocytes in vivo. The FEBS Journal 269: 19-28
Rozengurt E (2011) Protein kinase D signaling: multiple biological functions in health and disease. Physiology (Bethesda) 26: 23-33
Samuel VT, Shulman GI (2012) Mechanisms for insulin resistance: common threads and missing links. Cell 148: 852-71
Sassmann A, Offermanns S, Wettschureck N (2010) Tamoxifen-inducible Cre-mediated recombination in adipocytes. Genesis 48: 618-625
Schneider K, Valdez J, Nguyen J, Vawter M, Galke B, Kurtz TW, Chan JY (2016) Increased energy expenditure, Ucp1 expression, and resistance to diet-induced obesity in mice lacking nuclear factor-erythroid-2-related transcription factor-2 (Nrf2). Journal of Biological Chemistry 291: 7754-7766
Singh R, Xiang Y, Wang Y, Baikati K, Cuervo AM, Luu YK, Tang Y, Pessin JE, Schwartz GJ, Czaja MJ (2009) Autophagy regulates adipose mass and differentiation in mice. The Journal of clinical investigation 119: 3329-3339
Spiegelman BM, Flier JS (2001) Obesity and the regulation of energy balance. Cell 104: 531-43
Steiner TS, Ivison SM, Yao Y, Kifayet A (2010) Protein kinase D1 and D2 are involved in chemokine release induced by toll-like receptors 2, 4, and 5. Cell Immunol 264: 135-42
Subramanian A, Tamayo P, Mootha VK, Mukherjee S, Ebert BL, Gillette MA, Paulovich A, Pomeroy SL, Golub TR, Lander ES, Mesirov JP (2005) Gene set enrichment analysis: a knowledge-based approach for interpreting genome-wide expression profiles. Proceedings of the National Academy of Sciences of the United States of America 102: 15545-50
Sumara G, Formentini I, Collins S, Sumara I, Windak R, Bodenmiller B, Ramracheya R, Caille D, Jiang H, Platt KA, Meda P, Aebersold R, Rorsman P, Ricci R (2009) Regulation of PKD by the MAPK p38delta in insulin secretion and glucose homeostasis. Cell 136: 235-48
Sumara G, Sumara O, Kim JK, Karsenty G (2012) Gut-derived serotonin is a multifunctional determinant to fasting adaptation. Cell Metab 16: 588-600

Tanaka T, Yoshida N, Kishimoto T, Akira S (1997) Defective adipocyte differentiation in mice lacking the C/EBPβ and/or C/EBPδ gene. The EMBO journal 16: 7432-7443
Tol MJ, Ottenhoff R, van Eijk M, Zelcer N, Aten J, Houten SM, Geerts D, van Roomen C, Bierlaagh MC, Scheij S, Hoeksema MA, Aerts JM, Bogan JS, Dorn GW, 2nd, Argmann CA, Verhoeven AJ (2016) A PPARgamma-Bnip3 Axis Couples Adipose Mitochondrial Fusion-Fission Balance to Systemic Insulin Sensitivity. Diabetes 65: 2591-605
Toyama EQ, Herzig S, Courchet J, Lewis TL, Jr., Loson OC, Hellberg K, Young NP, Chen H, Polleux F, Chan DC, Shaw RJ (2016) Metabolism. AMP-activated protein kinase mediates mitochondrial fission in response to energy stress. Science 351: 275-281
Tozzi M, Novak I (2017) Purinergic receptors in adipose tissue as potential targets in metabolic disorders. Frontiers in pharmacology 8: 878
Trujillo Viera J, El-Merahbi R, Nieswandt B, Stegner D, Sumara G (2016) Phospholipases D1 and D2 Suppress Appetite and Protect against Overweight. PLoS One 11: e0157607
Twig G, Hyde B, Shirihai OS (2008) Mitochondrial fusion, fission and autophagy as a quality control axis: the bioenergetic view. Biochim Biophys Acta 1777: 1092-7
Wikstrom JD, Mahdaviani K, Liesa M, Sereda SB, Si Y, Las G, Twig G, Petrovic N, Zingaretti C, Graham A, Cinti S, Corkey BE, Cannon B, Nedergaard J, Shirihai OS (2014) Hormone-induced mitochondrial fission is utilized by brown adipocytes as an amplification pathway for energy expenditure. EMBO J 33: 418-36
Zechner R, Zimmermann R, Eichmann TO, Kohlwein SD, Haemmerle G, Lass A, Madeo F (2012) FAT SIGNALS--lipases and lipolysis in lipid metabolism and signaling. Cell Metab 15: 279-91
Zennaro M-C, Le Menuet D, Viengchareun S, Walker F, Ricquier D, Lombès M (1998) Hibernoma development in transgenic mice identifies brown adipose tissue as a novel target of aldosterone action. The Journal of clinical investigation 101: 1254-1260
Zhang Y, Goldman S, Baerga R, Zhao Y, Komatsu M, Jin S (2009) Adipose-specific deletion of autophagy-related gene 7 (atg7) in mice reveals a role in adipogenesis. Proceedings of the National Academy of Sciences 106: 19860-19865
Zhang Z, Zhang H, Li B, Meng X, Wang J, Zhang Y, Yao S, Ma Q, Jin L, Yang J, Wang W, Ning G (2014) Berberine activates thermogenesis in white and brown adipose tissue. Nat Commun 5: 5493
Zheng Q, Lin J, Huang J, Zhang H, Zhang R, Zhang X, Cao C, Hambly C, Qin G, Yao J (2017) Reconstitution of UCP1 using CRISPR/Cas9 in the white adipose tissue of pigs decreases fat deposition and improves thermogenic capacity. Proceedings of the National Academy of Sciences 114: E9474-E9482
Zhu Q, Ghoshal S, Rodrigues A, Gao S, Asterian A, Kamenecka TM, Barrow JC, Chakraborty A (2016) Adipocyte-specific deletion of Ip6k1 reduces diet-induced obesity by enhancing AMPK-mediated thermogenesis. J Clin Invest 126: 4273-4288

Figure 1 - PKD1 promotes triglyceride (TG) accumulation and lipogenesis in adipocytes.

A, B Quantification of relative TG accumulation using AdipoRed reagent (A) and images of Oil-Red-O staining for neutral lipids (B) in 3T3L1 cells differentiated into adipocytes depleted from PKD1 using shRNA (shPKD1) or corresponding non targeting control (shNTC) (n=6; representative of three individual experiments).

C, D Quantification of relative TG accumulation using AdipoRed reagent (C) and images of Oil-Red-O staining for neutral lipids (D) in 3T3L1 cells which have been differentiated after overexpressing of wild type form of PKD1 (PKD1wt) as well as constitutive active form of PKD1 (PKD1ca) and corresponding controls (Myc) (C and D) (n=6; representative of three individual experiments).

E-G Basal and insulin-induced lipogenesis rate (arbitrary units - AU) in differentiated 3T3L1 depleted of PKD1 by shRNA (E), PKD1-deficient adipocytes derived from SVC (F), and 3T3L1 cells expressing PKD1ca (G) (n=3; representative for three individual experiments).

Data information: In (A, C, E-G) data are presented as mean ± SEM. *$P < 0.05$ and ***$P < 0.001$ (one way ANOVA with Tukey's multiple comparisons post test (C) or unpaired, two-tailed Student's t-Test (A, E-G)).

Figure 2 – Deletion of PKD1 increases energy dissipation and mitochondrial fragmentation in adipocytes.

A. Oxygen consumption rate (OCR) in response to indicated substances as well as OCR annotated to the indicated cellular processes in PKD1-deficient SVC differentiated into adipocytes (n=14; representative of three individual experiments).

B. Ratio of mitochondrial (mtDNA) and genomic DNA (gDNA) in SVC-derived adipocytes with deletion of PKD1 (n=5; reperesentative of three individual experiments).

C. OCR upon indicated substances and OCR required for indicated processes in PKD1ca expressing 3T3L1 cells (n=30; representative of three individual experiments).

D, E Representative microscopy images of the mitochondrial morphology and its respective quantification in PKD1-deficient adipocytes derived from SVC (D) and differentiated 3T3L1 cells expressing PKD1ca (E).

Data information: In (A-E), data are presented as mean ± SEM. In (D, E), data represent three independent experiments with 200 cells counted for each replicate *P < 0.05, **P < 0.01, and ***P < 0.001 (unpaired, two-tailed Student's t-Test).

Figure 3 - PKD1 promotes lipogenesis, TG accumulation and suppresses OCR in an AMPK-dependent manner

A. Western blot (WB) analysis using antibodies against indicated proteins in protein lysates of differentiated 3T3-L1 cells lacking PKD1 and densitometric quantification 3 to 4 replicates for each protein.

B, C AMPK activity in differentiated 3T3L1 cells expressing PKD1ca (B) and 3T3L1 cells depleted PKD1 (C). Compound C (CC) stimulated cells served as a negative control (n>5; average of two individual experiments).

D, E Basal and insulin-induced lipogenesis rate (arbitrary units - AU) in differentiated 3T3L1 cells expressing PKD1ca treated with AICAR (2 mM) for 2 hour (D) and cells lacking PKD1 which have been transfected with control siRNA and siRNA against AMPKα1/α2 subunits (E) (n=3; representative of three individual experiments).

F. Basal and insulin-induced lipogenesis rate (arbitrary units - AU) in explants derived from subcutaneous white adipose tissue (sWAT) of control mice and mice lacking PKD1 treated with Compound C (CC) (5 μM) for 4 hours (n=4; representative of two individual experiments).

G, H Quantification of relative TG accumulation using AdipoRed reagent (G) and images of Oil-Red-O staining for neutral lipids (H) in differentiated 3T3L1 cells expressing PKD1ca and

corresponding controls treated with AICAR (0.5 mM) for 3 days (n=3; representative of three individual experiments).

I, J OCR required for indicated processes in PKD1-deficient 3T3l1 cells which have been transfected with control siRNA and siRNA against AMPKα1/α2 subunits (I) and PKD1ca expressing 3T3L1 cells treated with AICAR (0.5 mM) for 3 days (J)) (n=22; representative of two individual experiments).

Data information: In (A-G, I, and J), quantitative data are presented as mean ± SEM. *P < 0.05, **P < 0.01, and ***P < 0.001 (one way ANOVA with Tukey's multiple comparisons post test (C-G, I, and J) or unpaired, two-tailed Student's t-Test (A and B)).

Figure 4 – Deletion of PKD1 in adipocytes protects against obesity by increasing energy dissipation

A. WB analysis of indicated proteins in sWAT from 24 hours fasted and 24 hours fasted-refed mice including densitometric quantification of triplicates for each protein.

B. QPCR analysis of PKD1 expression in sWAT from fasted and fasted-refed mice (n = 3 mice per group).

C. Body weight evolution of control and PKD1adipoΔ/Δ mice fed HFD and ND (n>5/genotype).

D. Organ weight of control and PKD1adipoΔ/Δ mice fed HFD (n>8/genotype).

E-G Food intake (E), voluntary movement (F), and energy expenditure (G) of control and PKD1adipoΔ/Δ mice fed HFD (n>8/genotype).

H-L Representative H&E stains of gonadal white adipose tissue (gWAT) (H), interscapular brown adipose tissue (BAT) (J), and sWAT (K) from PKD1adipoΔ/Δ and control mice fed HFD. Average adipocyte size in (I) gWAT and (L) sWAT of indicated mice fed HFD (n=8/genotype).

Data information: In (A-G, I, and L), data are presented as mean ± SEM. *P < 0.05 and ***P < 0.001 (one way ANOVA with Tukey's multiple comparisons post test (C) or unpaired,

two-tailed Student's t-Test (A, B, D-G, I, and L)).

Figure 5 - PKD1 suppresses expression of genes characteristic for beiging.

A. RNA-sequencing based heat map of the expression patterns of browning-related genes in sWAT from mice of the indicated genotypes (GSE analysis software) (n=4/genotype).

B. MA-plot showing RNA-sequencing results. Differential expression and average abundance (indicated as log2 fold-change (FC) and log counts-per-million (CPM)) of all genes was calculated with EdgeR. Beiging related genes are highlighted in red (n=4/genotype).

C. QPCR analyzes of expression of indicated genes in sWAT from control and PKD1-deficient mice (n=6/genotype).

D. Ratio of mtDNA and gDNA in sWAT of control and PKD1-deficient mice (n=6/genotype).

E. WB analysis of UCP1 in sWAT from control and PKD1-deficient mice fed HFD including densitometric quantification of 4 replicates each.

Data information: In (C-E), data are presented as mean ± SEM. *$P < 0.05$ and **$P < 0.01$ (unpaired, two-tailed Student's t-Test).

Figure 6 - PKD1 suppresses ADRB3 expression in an AMPK – C/EBP-α/C/EBP-δ – dependent manner.

A. QPCR analyzes of expression of indicated genes in differentiated SVC derived from sWAT from control and PKD1-deficient mice (n>7).

B. Representative immunofluorescent images of ADRB3 staining and quantification of fluorescent intensity in PKD1-deficient and control adipocytes derived from SVC (n>43; representative of two individual experiments).

C. QPCR analyzes of *Ucp1* in differentiated SVC of indicated genotypes after 24 hours stimulation with Isoproterenol (Iso) at indicated concentrations (n=5, representative of two individual experiments).

D, E WB analysis of indicated proteins in differentiated 3T3L1 cells lacking PKD1 (D) and SVC from control and PKD1-deficient mice (E) including densitometric quantification of triplicates each.

F. WB analysis of indicated proteins in differentiated 3T3L1 expressing PKD1ca and treated with AICAR (2 mM) for 2 hours.

G QPCR analysis of *Adrb3* in SVC derived from sWAT of control and PKD1-deficient mice transfected with control siRNA, siRNA against C/EBP-α and/or C/EBP-δ (n>4).

Data information: In (A-G), data are presented as mean ± SEM. *P < 0.05, **P < 0.01 and ***P < 0.001 (one way ANOVA with Tukey's multiple comparisons post test (G) or unpaired, two-tailed Student's t-Test (A-E)).

Figure 7 - Deletion of PKD1 in adipocytes protects against peripheral insulin resistance and hepatic steatosis.

A-C FFAs levels (A), glucose (B), and insulin (C) tolerance test in PKD1adipoΔ/Δ and control mice fed ND or HFD (n>5/genotype).

D, E WB analysis of indicated proteins in SVC-derived adipocytes lacking PKD1 (D) and 3T3L1-derived adipocytes expressing PKD1ca (E).

F, G Oil-Red-O staining of liver sections (F) and liver TG content (G) from PKD1adipoΔ/Δ and control mice fed HFD (n>8/genotype).

H. Correlation between PKD1 expression and HOMA-IR levels in human sWAT.

I. Basal and insulin-induced lipogenesis rate (arbitrary units - AU) in differentiated human subcutaneous preadipocytes treated with CRT 0066101 (3 μM) or vehicle for 3 days (n=4; representative of two individual experiments).

J. Oxygen consumption rate (OCR) in response to indicated substances as well as OCR annotated to the indicated cellular processes in differentiated human subcutaneous preadipocytes treated with CRT 0066101 (3 μM) for 3 days (n=19; representative of two individual experiments).

Data information: In (A-C, G, I and J), data are presented as mean ± SEM. *P < 0.05, **P < 0.01 and ***P < 0.001 (one way ANOVA with Tukey's multiple comparisons post test (A-C) or unpaired, two-tailed Student's t-Test (G, I, and J)).

Figure 8 – Inactivation of PKD1 in obese mice prevents further body weight gain

A. Body weight evolution of control and tamoxifen-inducible PKD1 deletion (PKD1ind.adipoΔ/Δ) mice fed HFD for 22 weeks (n>6/genotype).

B. Fat mass gain after tamoxifen injection in control and PKD1ind.adipoΔ/Δ mice fed HFD (n>6/genotype).

C-E Energy expenditure (C), voluntary movement (D), and food intake (E) of control and PKD1ind.adipoΔ/Δ mice fed HFD (n>6/genotype).

F. Glucose tolerance test in PKD1ind.adipoΔ/Δ and control mice after 17 weeks of HFD (n>6/genotype).

Data information: In (A-F), data are presented as mean ± SEM. *P < 0.05 and ***P < 0.001 (unpaired, two-tailed Student's t-Test).

Figure EV1 – Extracellular purines (ATP and ADP) promotes PKD1 activity

A. Western blot (WB) analysis of levels of indicated proteins in undifferentiated 3T3L1 cells and 3T3L1 cells differentiated into adipocytes stimulated with DAG (100 μM) for indicated time points.

B. DAG content measured in subcutaneous white adipose tissue (sWAT) and brown adipose tissue (BAT) of wild-type mice fed HFD or ND (n=6/genotype).

C-E WB analysis using indicated antibodies in differentiated 3T3L1 cells stimulated with the indicated substances for the given time points.

F. WB analysis using indicated antibodies in explants from sWAT of wild-type mice treated with different concentrations of ATP for the given time points.

G-I. WB analysis of levels of indicated proteins in differentiated T3TI cells which have been stimulated with the indicated substances for the given time points.

Data information: In (B), data are presented as mean ± SEM. (unpaired, two-tailed Student's t-Test).

Figure EV2 - PKD1 promotes mitochondrial aggregation in an AMPK-dependent manner.

Representative microscopy images of the mitochondrial morphology and its respective quantification in differentiated 3T3L1 cells expressing PKD1ca, which have been treated with AICAR (2 mM) for 2 hours. Data are presented as mean ± SEM. Data represent three independent experiments with 200 cells counted for each replicate. *$P < 0.05$ (unpaired, two-tailed Student's t-Test).

Figure EV3 - PKD1 deletion promotes AMPK signaling in adipose tissue of mice fed ND

A. WB analysis of indicated proteins in sWAT of control and PKD1-deficient mice fed ND including densitometric quantification of 3 to 4 replicates each.

B-E. FFA (B), Glycerol (C), TG (D), and glucose (E) levels in blood of PKD1adipoΔ/Δ and control mice after 24 hours fasting and 24 hours fasting-refeeding (n>5/genotype).

Data information: In (A-E), data are presented as mean ± SEM. *P < 0.05, **P < 0.01, and ***P < 0.001 (unpaired, two-tailed Student's t-Test).

Figure EV4 - PKD1 deletion in adipocytes does not affect AMPK signaling in BAT.

A, B WB analysis of indicated proteins in sWAT of control and PKD1-deficient mice fed HFD (A) and BAT of the same mice fed ND and HFD (B) including densitometric quantification of 4 replicates each (A, B).

Data information: In (A, B), data are presented as mean ± SEM. *P < 0.05 (unpaired, two-tailed Student's t-Test).

Figure EV5 –PKD1 attenuates C/EBP-α and C/EBP-δ abundance.

A. WB analysis of indicated proteins in differentiated 3T3L1 cells expressing PKD1ca including densitometric quantification of 4 replicates each.

B, C QPCR analysis of *C/ebp-α* (B) and *C/ebp-δ* (C) in SVC derived from sWAT of control and PKD1-deficient mice transfected with control siRNA, siRNA against C/EBP-α and/or C/EBP-δ (n>4).

Data information: In (A-C), data are presented as mean ± SEM. *P < 0.05, **P < 0.01, and ***P < 0.001 (one way ANOVA with Tukey's multiple comparisons post test (B and C) or unpaired, two-tailed Student's t-Test (A)).

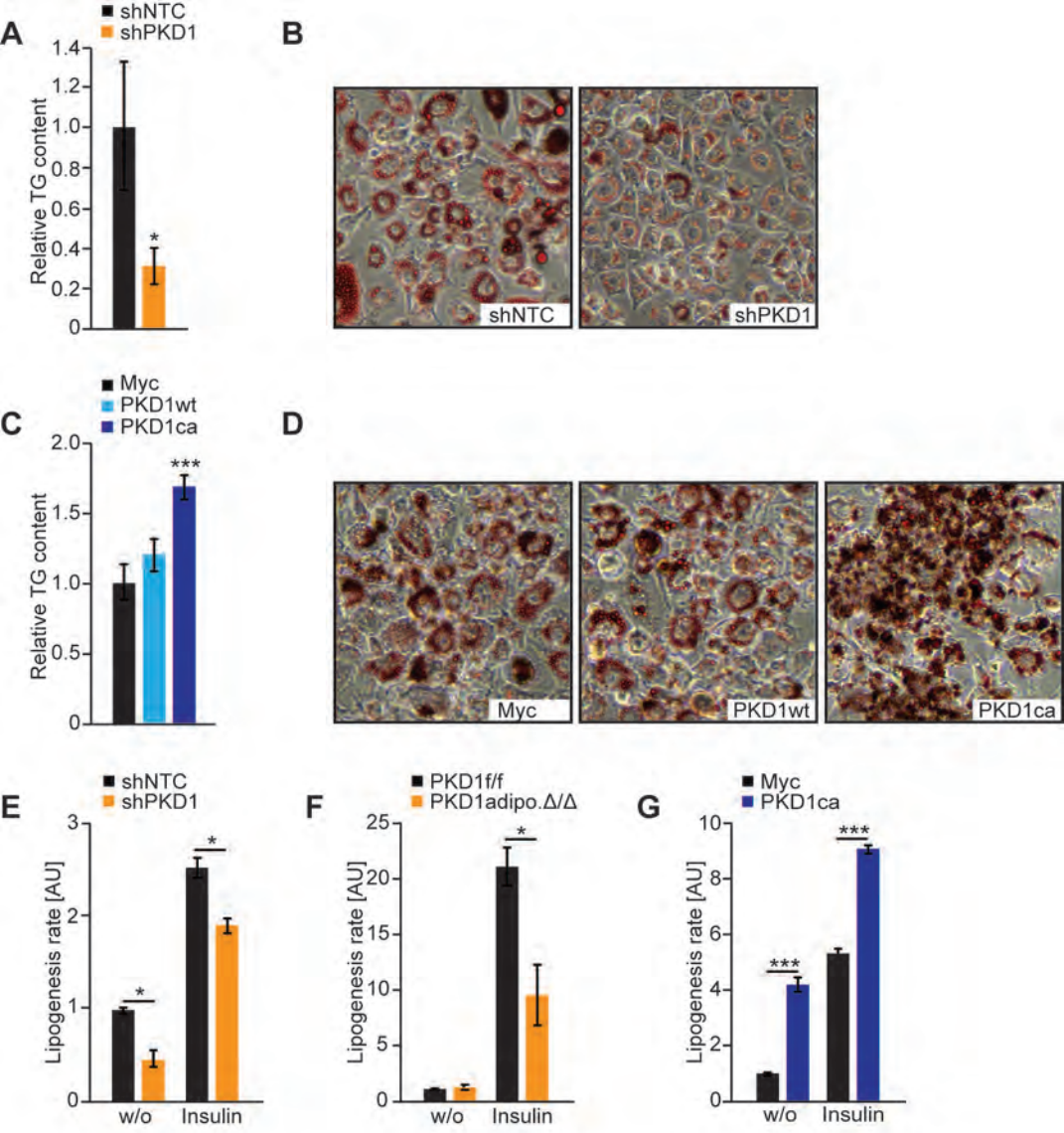
A
shNTC
shPKD1
Relative TG content
1.4
1.2
1.0
0.8
0.6
0.4
0.2
0
*
B
shNTC
shPKD1
C
Myc
PKD1wt
PKD1ca
Relative TG content
2.0
1.5
1.0
0.5
0
***
D
Myc
PKD1wt
PKD1ca
E
shNTC
shPKD1
Lipogenesis rate [AU]
3
2
1
0
*
*
w/o
Insulin
F
PKD1f/f
PKD1adipo.Δ/Δ
Lipogenesis rate [AU]
25
20
15
10
5
0
*
w/o
Insulin
G
Myc
PKD1ca
Lipogenesis rate [AU]
10
8
6
4
2
0
***
***
w/o
Insulin

Figure 1

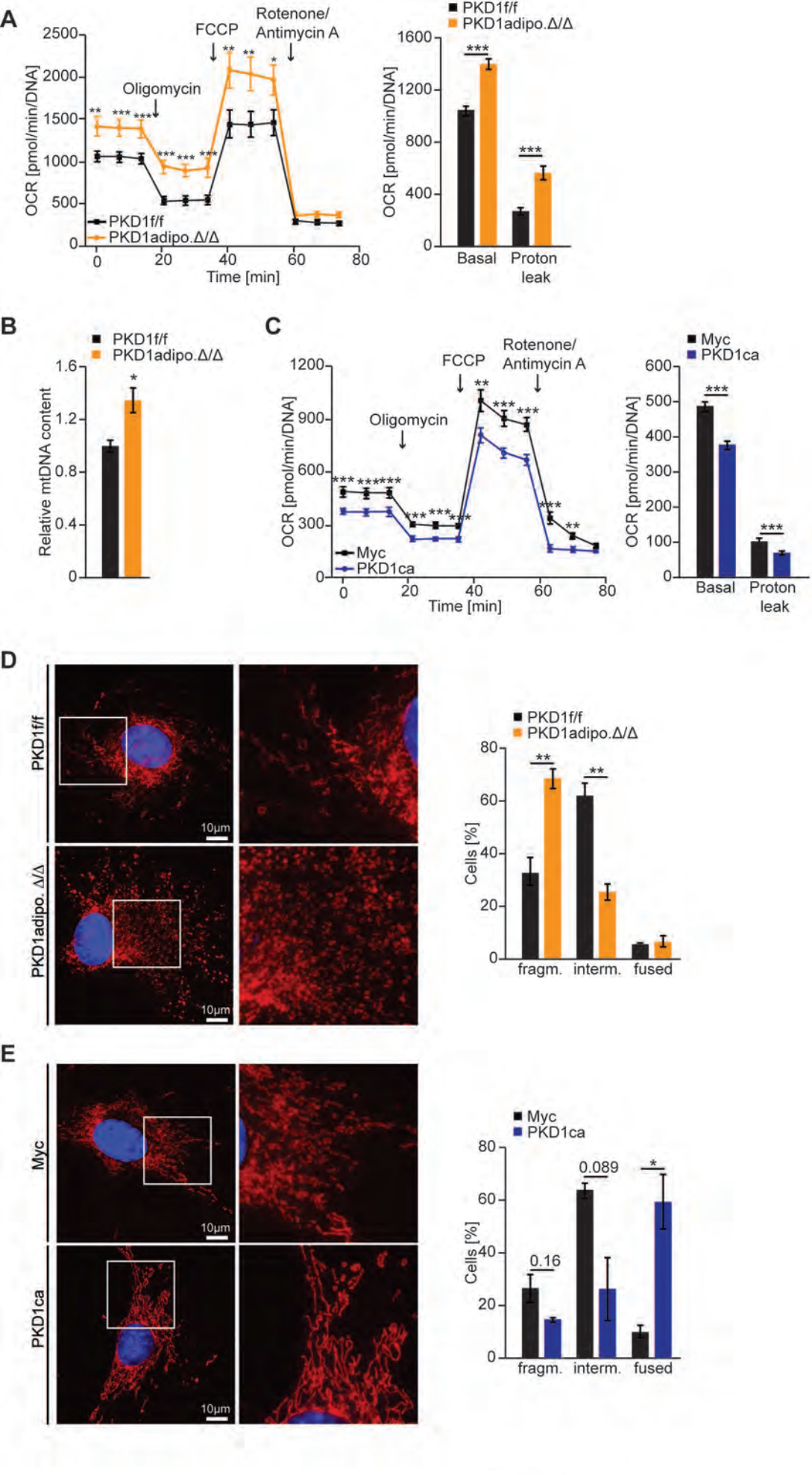
A
OCR [pmol/min/DNA]
Time [min]
Oligomycin
FCCP
Rotenone/
Antimycin A
PKD1f/f
PKD1adipo.Δ/Δ
Basal
Proton
leak
B
Relative mtDNA content
C
Myc
PKD1ca
D
PKD1f/f
PKD1adipo. Δ/Δ
10µm
Cells [%]
fragm.
interm.
fused
E
Myc
PKD1ca
0.16
0.089

Figure 2

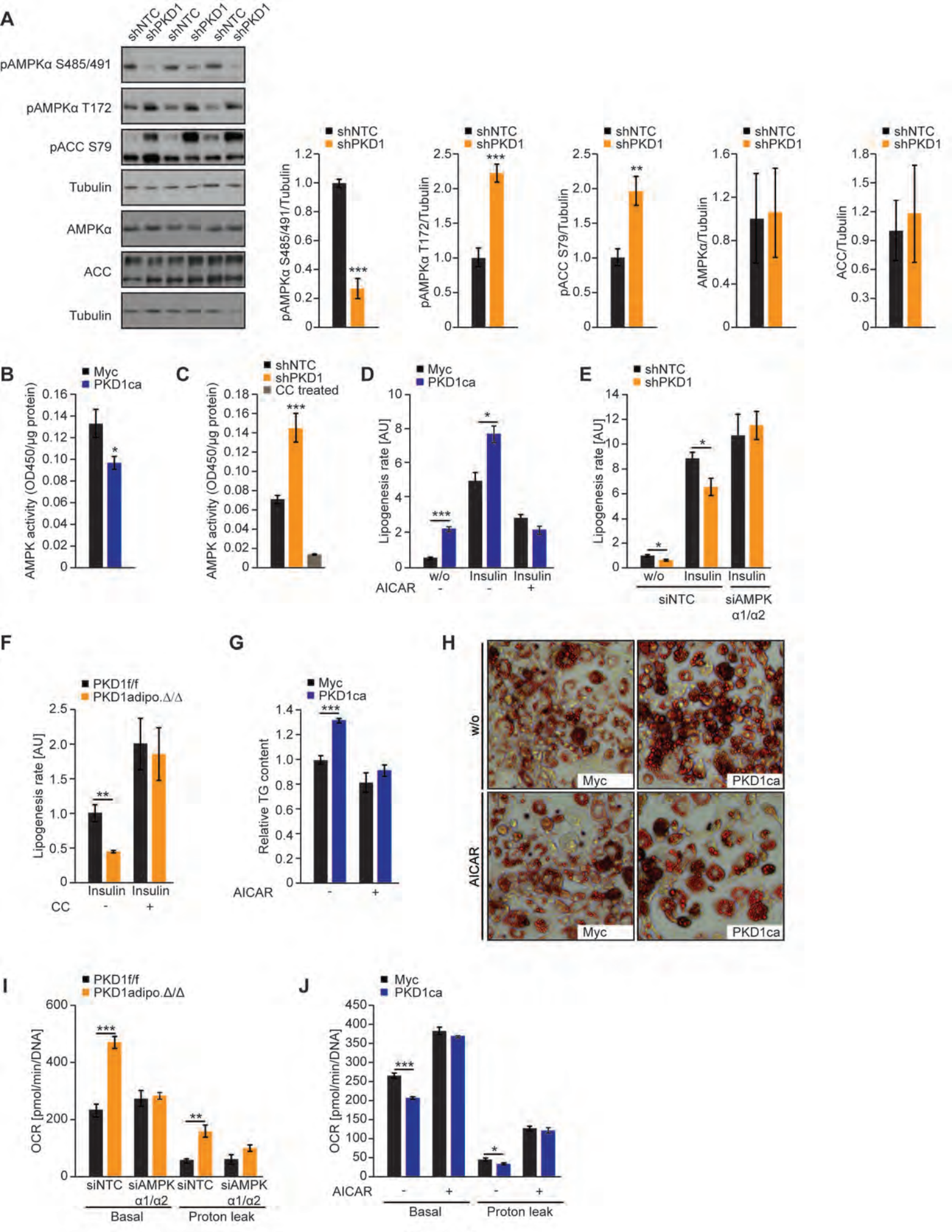
A
shNTC
shPKD1
pAMPKα S485/491
pAMPKα T172
pACC S79
Tubulin
AMPKα
ACC
Tubulin
pAMPKα S485/491/Tubulin
pAMPKα T172/Tubulin
pACC S79/Tubulin
AMPKα/Tubulin
ACC/Tubulin
B
Myc
PKD1ca
AMPK activity (OD450/µg protein)
C
CC treated
D
Lipogenesis rate [AU]
AICAR
w/o
Insulin
E
siNTC
siAMPK α1/α2
F
PKD1f/f
PKD1adipo.Δ/Δ
CC
G
Relative TG content
H
w/o
AICAR
I
OCR [pmol/min/DNA]
Basal
Proton leak
J

Figure 3

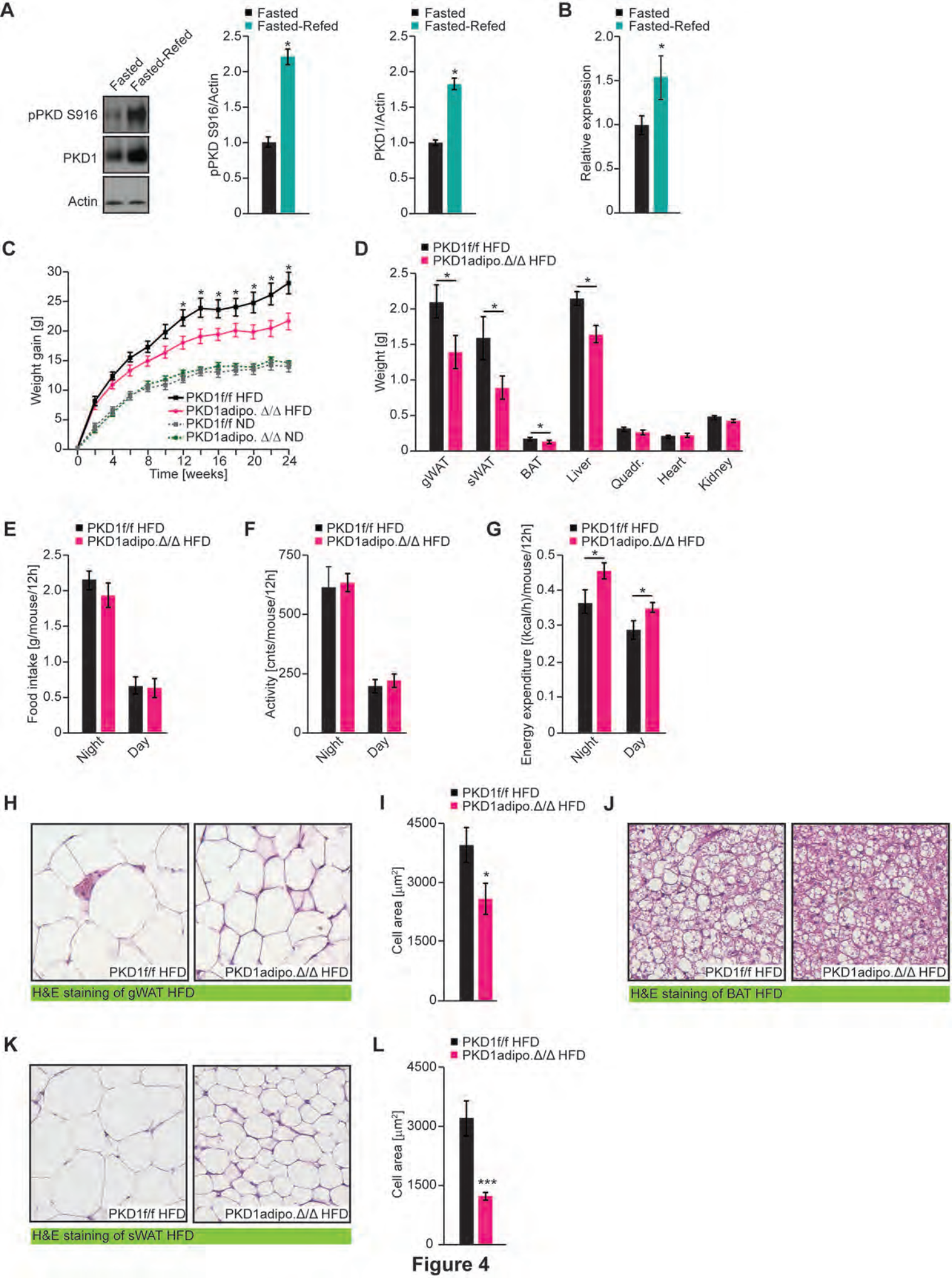
A
Fasted
Fasted-Refed
pPKD S916
PKD1
Actin
pPKD S916/Actin
PKD1/Actin
B
Relative expression
C
Weight gain [g]
Time [weeks]
PKD1f/f HFD
PKD1adipo. Δ/Δ HFD
PKD1f/f ND
PKD1adipo. Δ/Δ ND
D
PKD1f/f HFD
PKD1adipo.Δ/Δ HFD
Weight [g]
gWAT
sWAT
BAT
Liver
Quadr.
Heart
Kidney
E
Food intake [g/mouse/12h]
Night
Day
F
Activity [cnts/mouse/12h]
G
Energy expenditure [(kcal/h)/mouse/12h]
H
PKD1f/f HFD
PKD1adipo.Δ/Δ HFD
H&E staining of gWAT HFD
I
Cell area [μm²]
J
H&E staining of BAT HFD
K
H&E staining of sWAT HFD
L

Figure 4

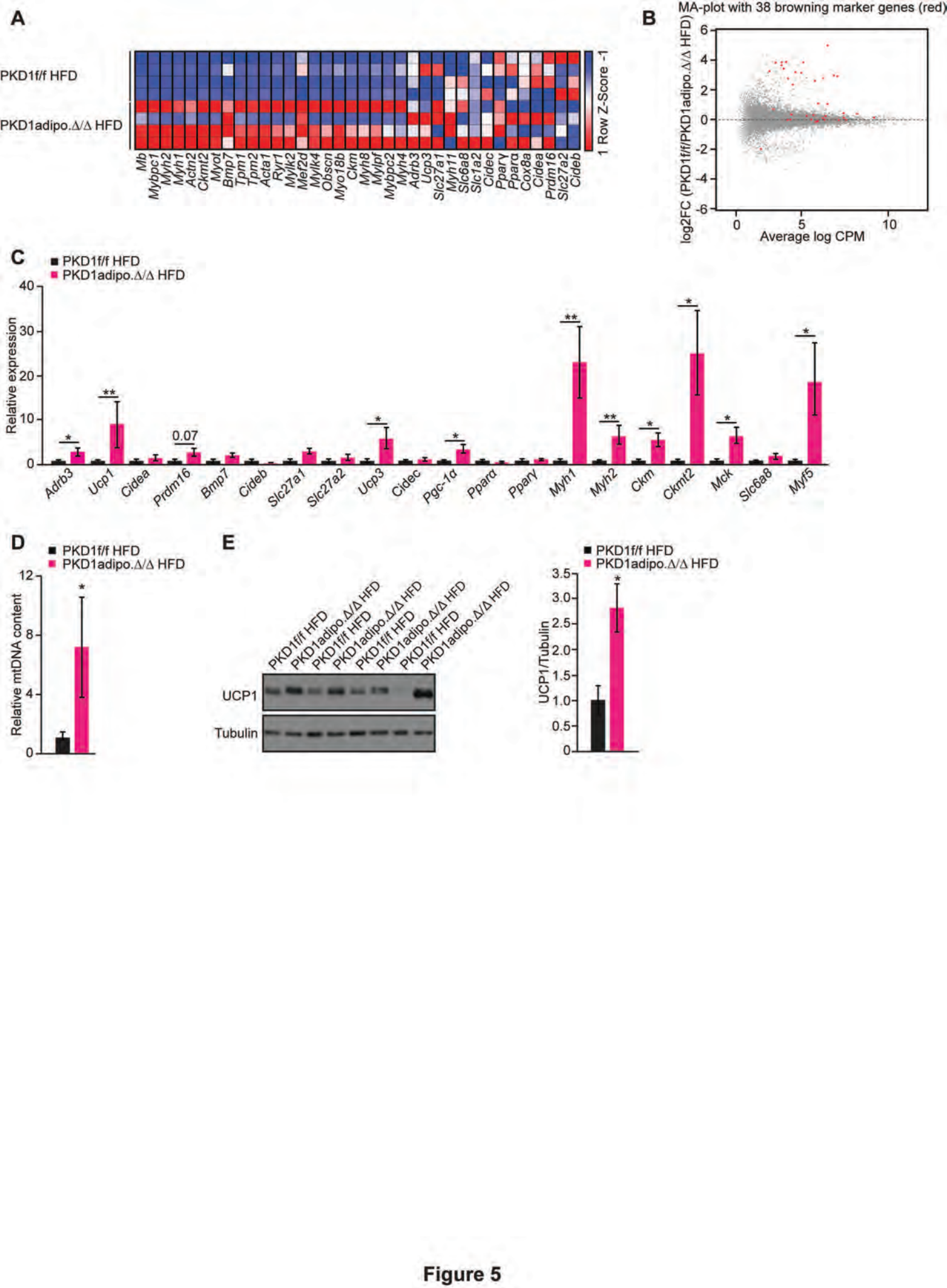
A
PKD1f/f HFD
PKD1adipo.Δ/Δ HFD
1 Row Z-Score -1
Mb
Mybpc1
Myh2
Myh1
Actn2
Ckmt2
Myot
Bmp7
Tpm1
Tpm2
Acta1
Ryr1
Mylk2
Mef2d
Mylk4
Obscn
Myo18b
Ckm
Myh8
Mylpf
Mybpc2
Myh4
Adrb3
Ucp3
Slc27a1
Myh11
Slc6a8
Slc1a2
Cidec
Pparγ
Pparα
Cox8a
Cidea
Prdm16
Slc27a2
Cideb
B
MA-plot with 38 browning marker genes (red)
log2FC (PKD1f/f/PKD1adipo.Δ/Δ HFD)
Average log CPM
C
PKD1f/f HFD
PKD1adipo.Δ/Δ HFD
Relative expression
0.07
Adrb3
Ucp1
Cidea
Prdm16
Bmp7
Cideb
Slc27a1
Slc27a2
Ucp3
Cidec
Pgc-1α
Pparα
Pparγ
Myh1
Myh2
Ckm
Ckmt2
Mck
Slc6a8
Myl5
D
PKD1f/f HFD
PKD1adipo.Δ/Δ HFD
Relative mtDNA content
E
PKD1f/f HFD
PKD1adipo.Δ/Δ HFD
UCP1
Tubulin
PKD1f/f HFD
PKD1adipo.Δ/Δ HFD
UCP1/Tubulin

Figure 5

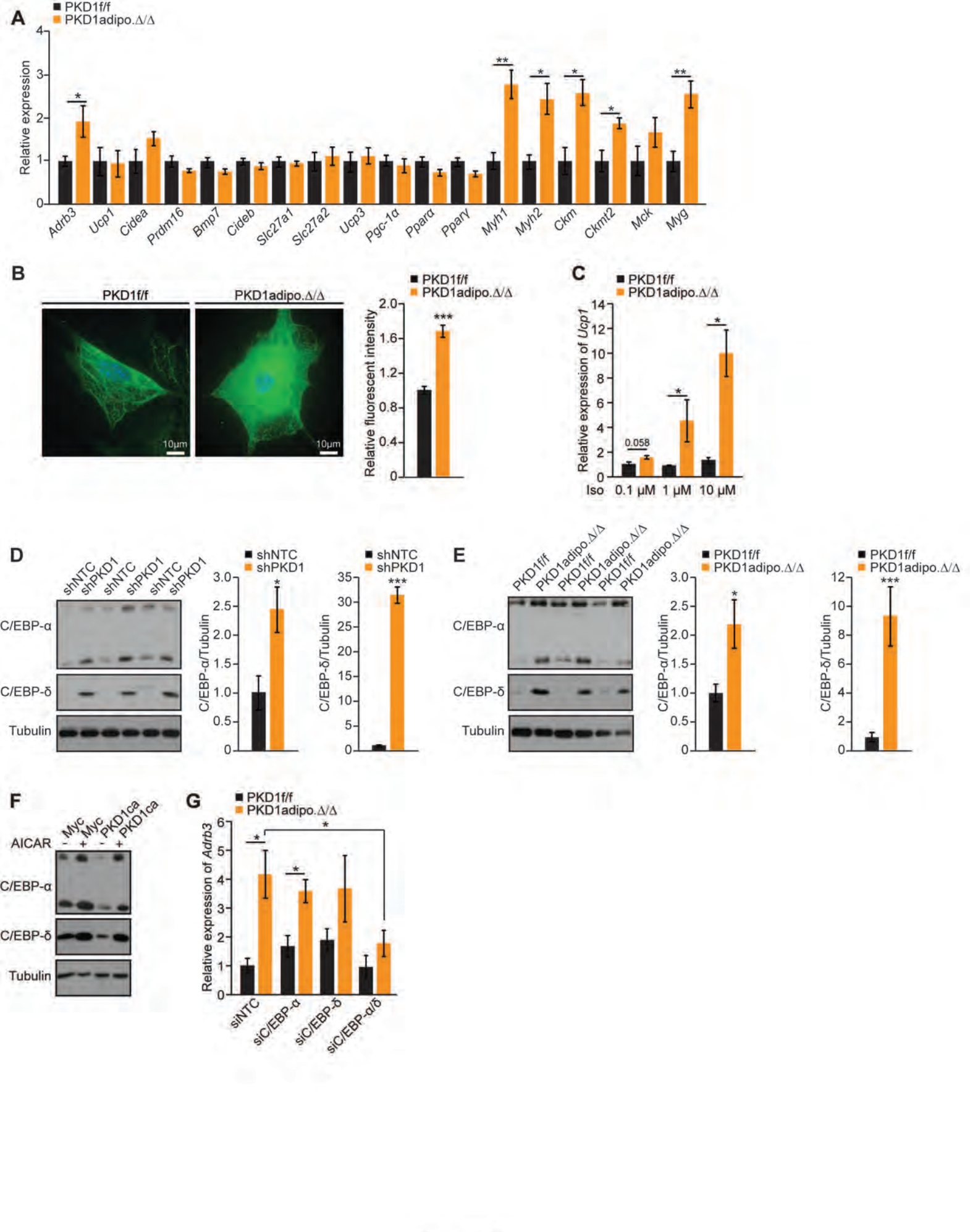
A
PKD1f/f
PKD1adipo.Δ/Δ
Relative expression
Adrb3
Ucp1
Cidea
Prdm16
Bmp7
Cideb
Slc27a1
Slc27a2
Ucp3
Pgc-1α
Pparα
Pparγ
Myh1
Myh2
Ckm
Ckmt2
Mck
Myg
B
PKD1f/f
PKD1adipo.Δ/Δ
10μm
Relative fluorescent intensity
C
Relative expression of Ucp1
0.058
Iso
0.1 μM
1 μM
10 μM
D
shNTC
shPKD1
C/EBP-α
C/EBP-δ
Tubulin
C/EBP-α/Tubulin
C/EBP-δ/Tubulin
E
PKD1f/f
PKD1adipo.Δ/Δ
F
Myc
PKD1ca
AICAR
G
Relative expression of Adrb3
siNTC
siC/EBP-α
siC/EBP-δ
siC/EBP-α/δ

Figure 6

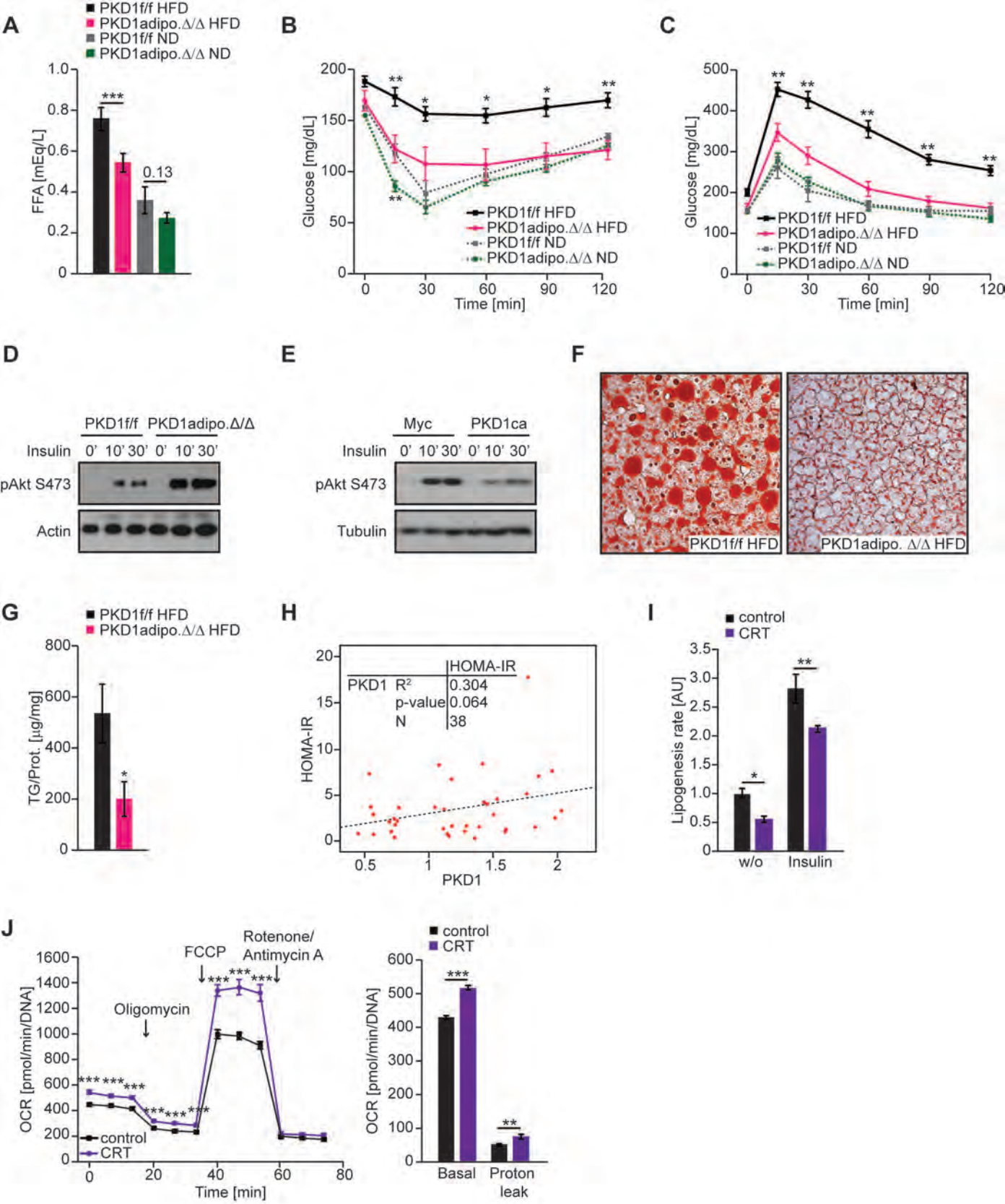
A
PKD1f/f HFD
PKD1adipo.Δ/Δ HFD
PKD1f/f ND
PKD1adipo.Δ/Δ ND
FFA [mEq/L]
0.13
B
Glucose [mg/dL]
Time [min]
C
Glucose [mg/dL]
Time [min]
D
PKD1f/f
PKD1adipo.Δ/Δ
Insulin
0' 10' 30' 0' 10' 30'
pAkt S473
Actin
E
Myc
PKD1ca
Insulin
0' 10' 30' 0' 10' 30'
pAkt S473
Tubulin
F
PKD1f/f HFD
PKD1adipo. Δ/Δ HFD
G
PKD1f/f HFD
PKD1adipo.Δ/Δ HFD
TG/Prot. [µg/mg]
H
HOMA-IR
PKD1 R²
p-value
N
0.304
0.064
38
HOMA-IR
PKD1
I
control
CRT
Lipogenesis rate [AU]
w/o
Insulin
J
FCCP
Rotenone/
Antimycin A
Oligomycin
OCR [pmol/min/DNA]
control
CRT
Time [min]
Basal
Proton
leak

Figure 7

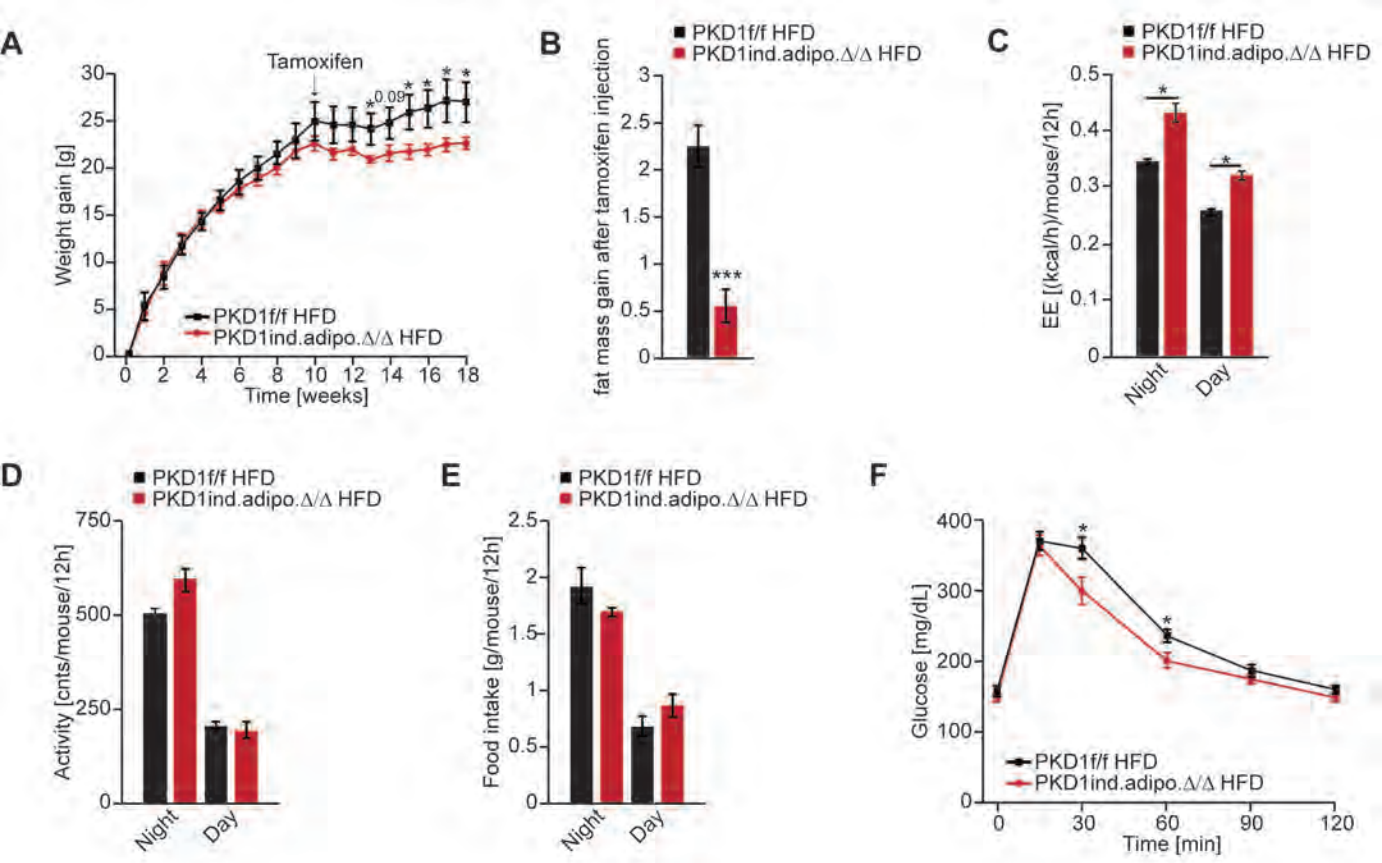
A
Tamoxifen
Weight gain [g]
Time [weeks]
PKD1f/f HFD
PKD1ind.adipo.Δ/Δ HFD
0.09
B
fat mass gain after tamoxifen injection
***
C
EE [(kcal/h)/mouse/12h]
Night
Day

D
Activity [cnts/mouse/12h]
E
Food intake [g/mouse/12h]
F
Glucose [mg/dL]
Time [min]

Figure 8

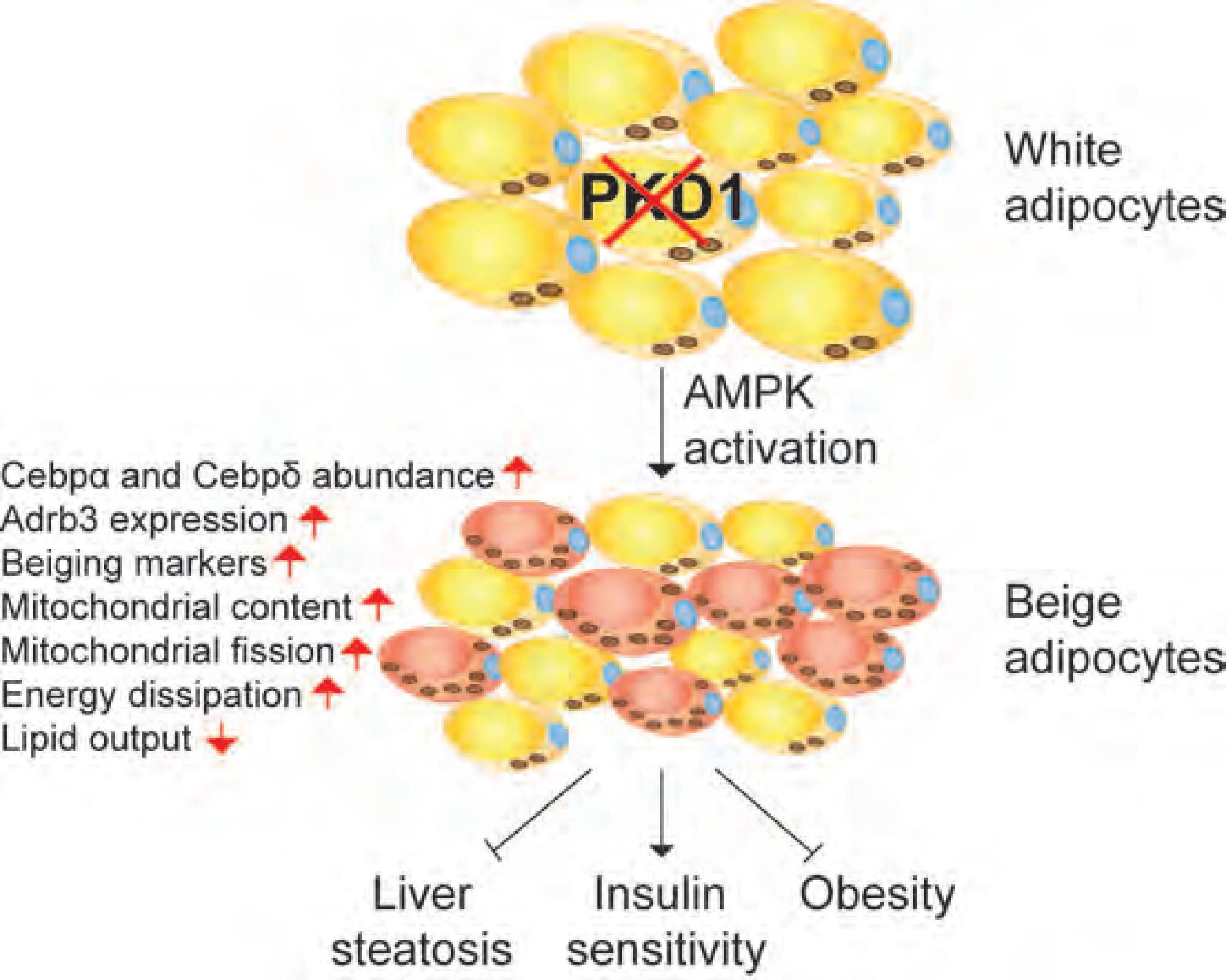
PKD1
White adipocytes
AMPK activation
Cebpα and Cebpδ abundance
Adrb3 expression
Beiging markers
Mitochondrial content
Mitochondrial fission
Energy dissipation
Lipid output
Beige adipocytes
Liver steatosis
Insulin sensitivity
Obesity

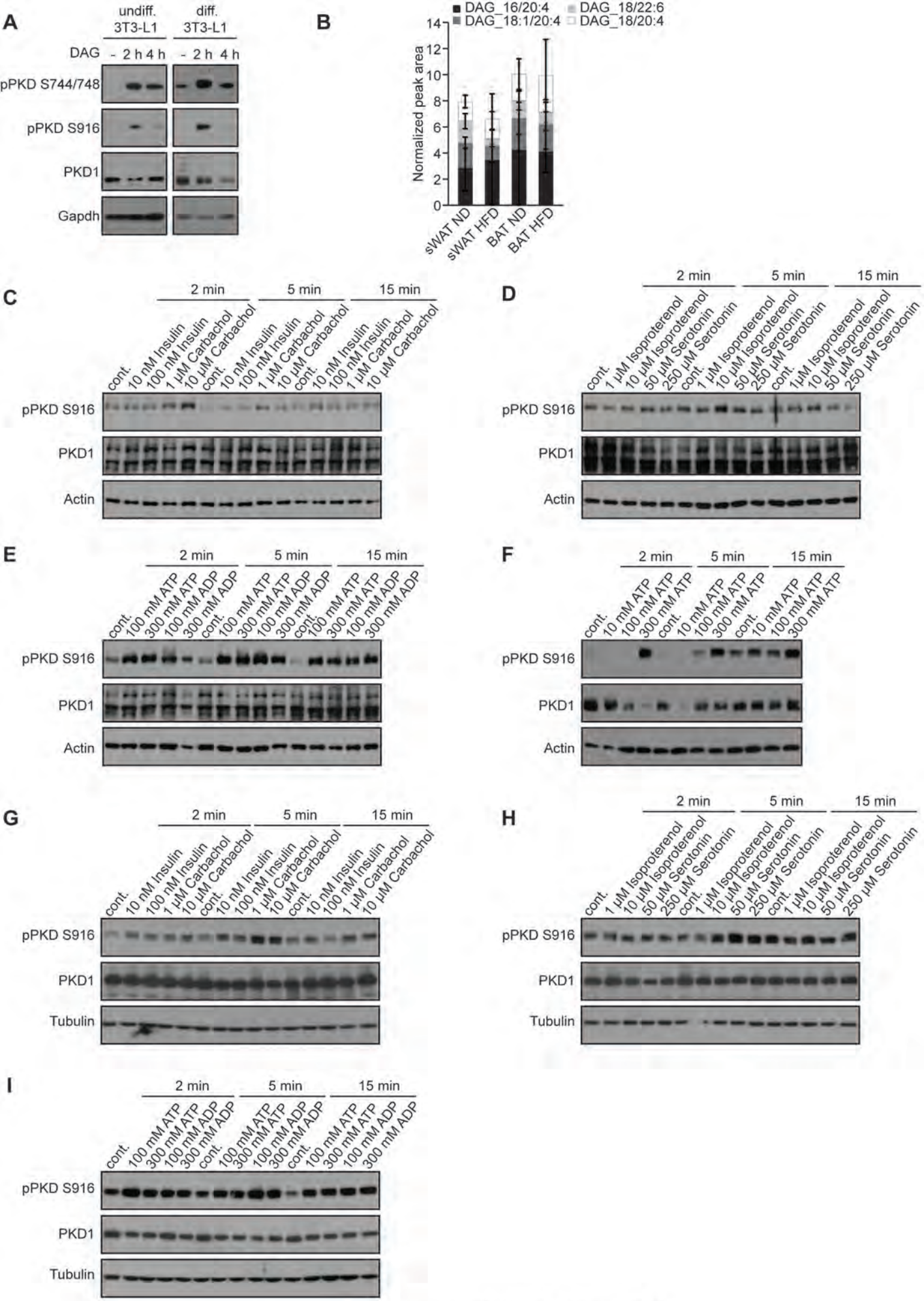

Expanded View - Figure EV1

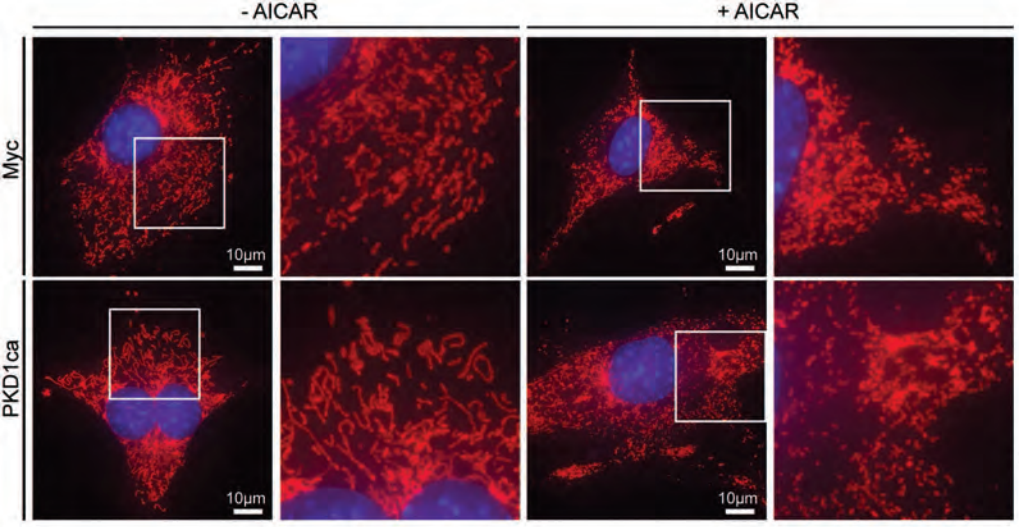

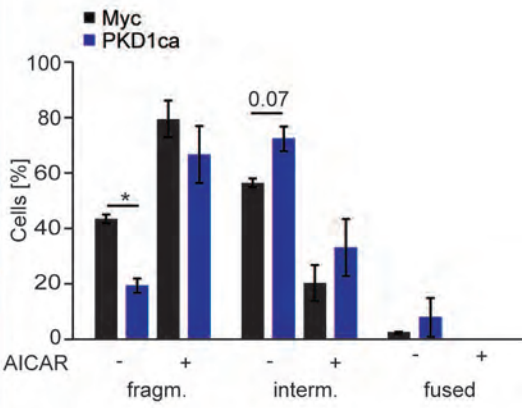

Expanded view- Figure EV2

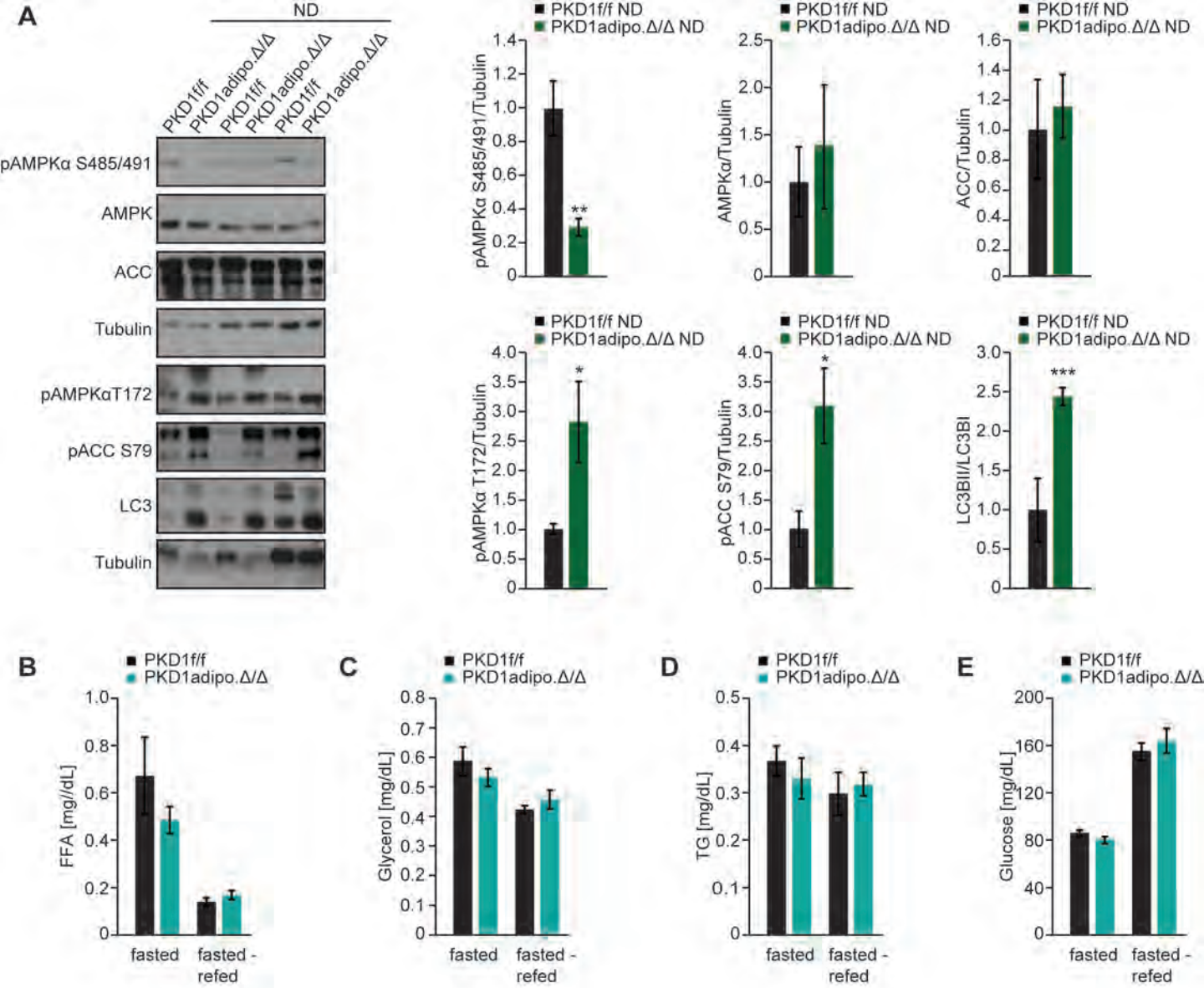

Expanded view - Figure EV3

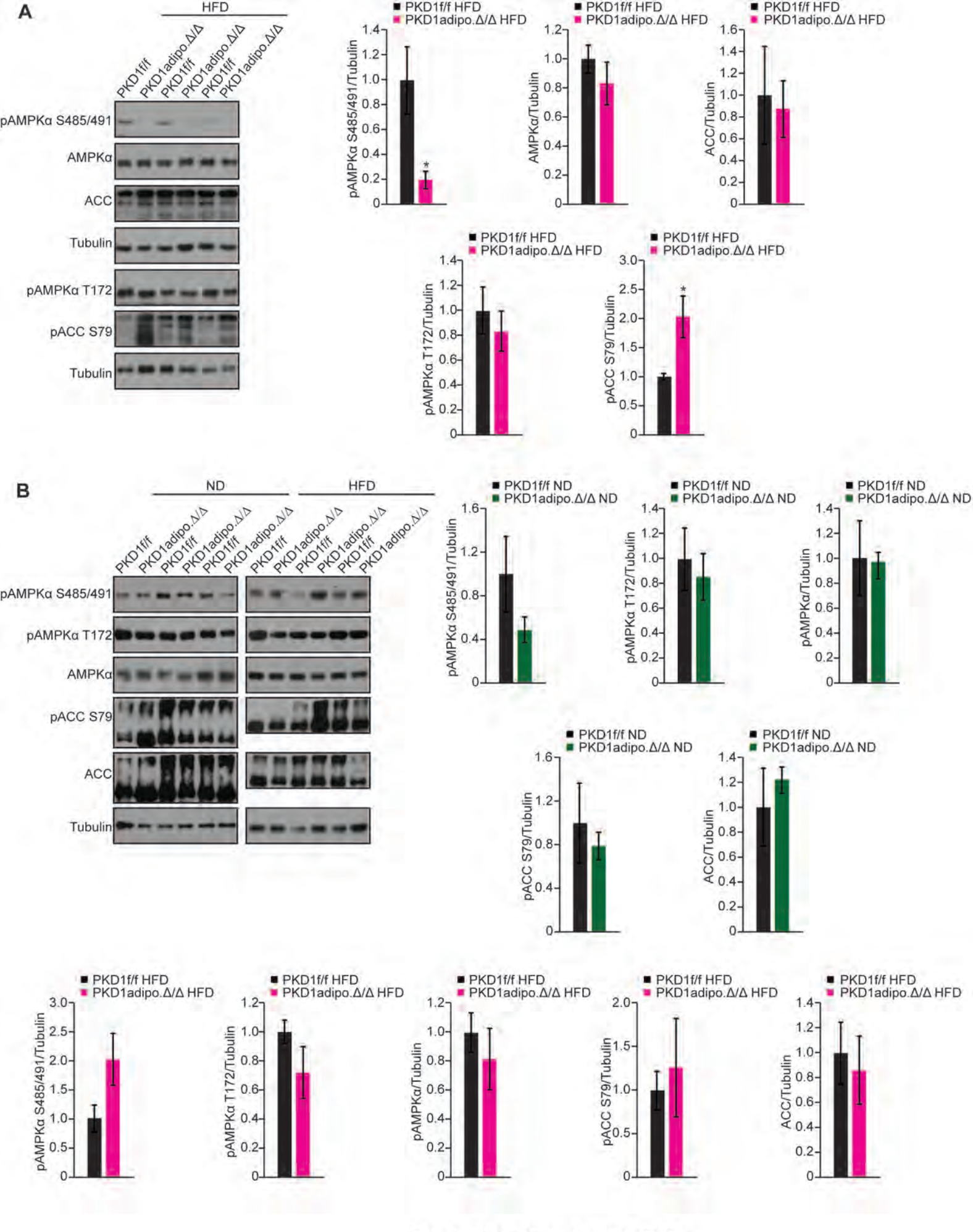

Expanded view - Figure EV4

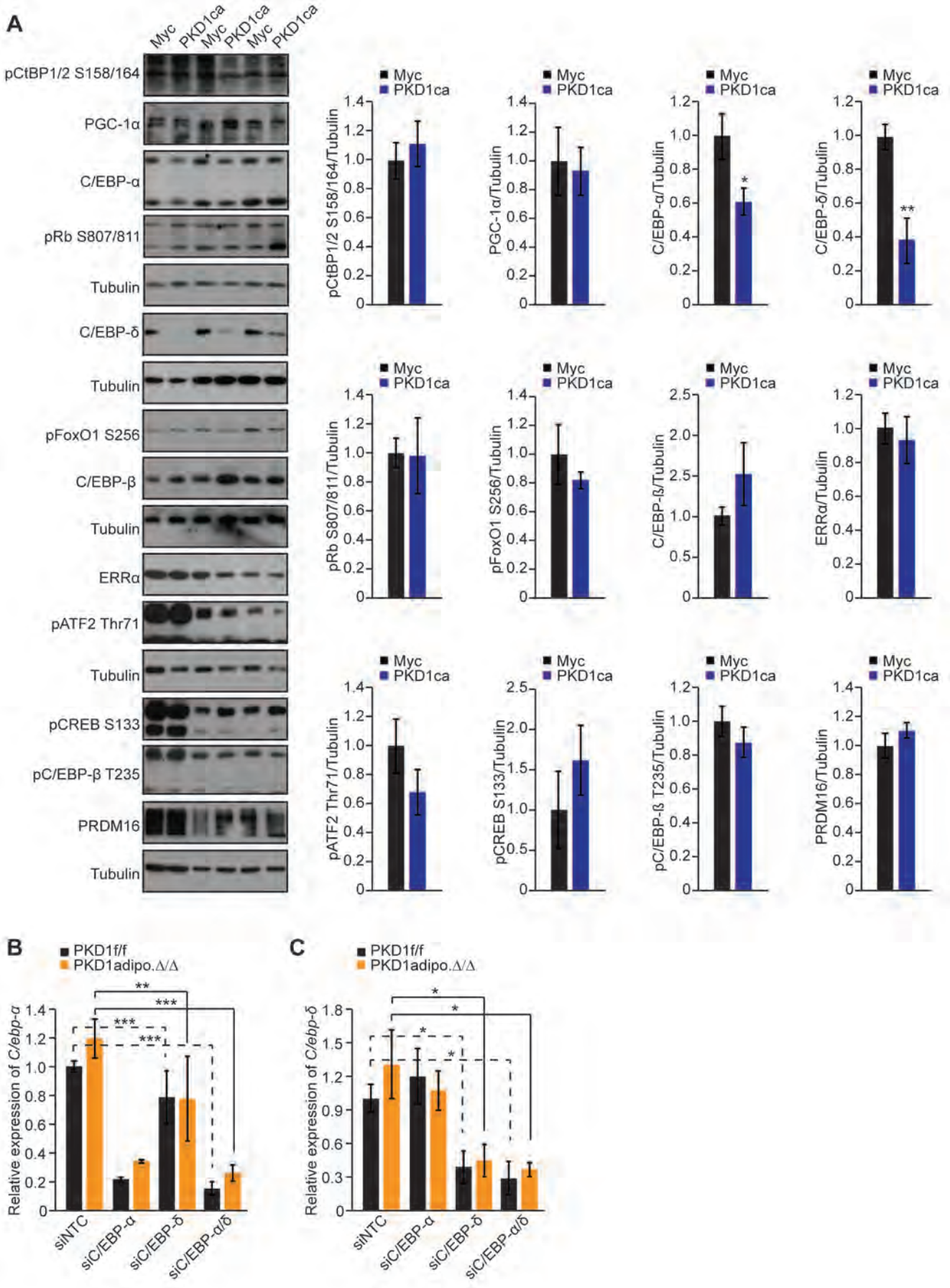

Expanded view - Figure EV5

Annex (Supplementary Material) to:

Protein kinase D1 deletion in adipocytes enhances energy dissipation and protects against adiposity

Table of Contents

Appendix - Table S1 - Sequences of the primers used for genotyping or Real-Time PCR.

Gene Name	Forward (5'-3')	Reverse (5'-3')
Cre Transgene	GGA TGT GCC ATG TGA GTC TG	ACG GAC AGA AGC ATT TTC CA
oIMR control	CTA GGC CAC AGA ATT GAA AGA TCT	GTA GGT GGA AAT TCT AGC ATC ATC C
PKD1flox	AGC TTC ACT TGG AAT GAC AC	GGT TGC ATG ATT TGT GAT AG
WT	CCG CAT CTT CTT GTG CAG T	ATC ACG TCC TCC ATC ATC C
Cre-ERT	GAG TCT GCC TTT CCC ATG AC	TCC CTC ACA TCC TCA GGT TC
Mt-CO1	TGCGCCGCAGGCATTAC	GGGTGCCCAAAGAATCAGAAC
Ndufv	CTTCCCCACTGGCCTCAAG	CCAAAACCCAGTGATCCAGC
Pkd1 Ex.16-17	CCCTCAGGTGAAGCTCTGTG	ACTTCAGGTGCCAGGTATGC
Pkd1 Ex.1-2	GGG GGC ATC TCG TTC CAT C	GTG CCG AAA AAG CAG GAT CTT
Pkd1 seq3	CCG TGA GAA GAG GTC AAA TTC G	GTG GCA CCT TCA CCT TAG ACA
Adrb3	GAT CTG GTC ATG GGA TTG CT	AAG TCC AGA GCT CGC AGA AG
Ucp1	AGG CTT CCA GTA CCA TTA GGT	CTG AGT GAG GCA AAG CTG ATT T
Cidea	TGACATTCATGGGATTGCAGAC	GGCCAGTTGTGATGACTAAGAC
Prdm16	CCACCAGCGAGGACTTCAC	GGAGGACTCTCGTAGCTCGAA
Bmp7	ACGGACAGGGCTTCTCCTAC	ATGGTGGTATCGAGGGTGGAA
Cideb	CAATGGCCTGCTAAGGTCAGT	GATCACAGACACGGAAGGGTC
Slc27a1	CGCTTTCTGCGTATCGTCTG	GATGCACGGGATCGTGTCT
Slc27a2	TCCTCCAAGATGTGCGGTACT	TAGGTGAGCGTCTCGTCTCG
Ucp3	CTGCACCGCCAGATGAGTTT	ATCATGGCTTGAAATCGGACC
Cidec	ATGGACTACGCCATGAAGTCT	CGGTGCTAACACGACAGGG
Pgc-1α	AGC GCC GTG TGA TTT ACG TT	CCG CAG ATT TAC GGT GCA TT
Pparα	AACATCGAGTGTCGAATATGTGG	CCGAATAGTTCGCCGAAAGAA
Pparγ	GGAAGACCACTCGCATTCCTT	GTAATCAGCAACCATTGGGTCA
Myh1	TCT GCA GAC GGA GTC AGG T	TTG AGT GAA TGC CTG TTT GC
Myh2	AAA GCT CCA AGG ACC CTC TT	AGC TCA TGA CTG CTG AAC TCA C
Ckm	CAG CAC AGA CAG ACA CTC AGG	GAA CTT GTT GTG GGT GTT GC
Ckmt2	GCA TGG TGG CTG GTG ATG AG	AAA CTG CCC GTG AGT AAT CTT
Mck	GCA AGC ACC CCA AGT TTG A	ACC TGT GCC GCG CTT CT
Scl6a8	TGC ATA TCT CCA AGG TGG CAG	CTA CAA ACT GGC TGT CCA GA
Myf5	CAG CCC CAC CTC CAA CTG	GGG ACC AGA CAG GGC TGT TA
Myg	AGC GCA GGC TCA AGA AAG TGA ATG	CTG TAG GCG CTC AAT GTA CTG GAT
Fasn	GGAGGTGGTGATAGCCGGTAT	TGGGTAATCCATAGAGCCCAG
Dgat	GTG CCA TCG TCT GCA AGA TT	CTG GAT AGG ATC CAC CAG GA
Lpl	GGGAGTTTGGCTCCAGAGTTT	TGTGTCTTCAGGGGTCCTTAG
Acc	GA CAG ACT GAT CGC AGA GAA AG	TGG AGA GCC CCA CAC ACA
Screbp1	GGA GCC ATG GAT TGC ACA TT	GGC CCG GGA AGT CAC TGT

Screbp2	GCGTTCTGGAGACCATGGA	ACAAAGTTGCTCTGAAAACAAATCA
Creb	TCGTGCCAGTGCGAGTGT	AGCCACGCGGGATGC
Chrebp	GTTCAGCATCCTCATCCGAC	GGAAGTGCTGAGTTGGCGAAG
Cebpα	AAACAACGCAACGTGGAGA	GCGGTCATTGTCACTGGTC
Cebpδ	TCAAATCCCTGCCCAAAGTG	CTGCAGAGGGCAAAGATCAC
Rpl13a	CCC TCC ACC CTA TGA CAA GA	GCC CCA GGT AAG CAA ACT T

Appendix - Table S2 - Characteristics of human subjects and blood analysis

Variables are presented as mean (standard deviation) or absolute frequency (percentage) and are compared by means of Mann-Whitney U test or $\chi 2$ test (see methods part).

Variable	Obese patients (n = 41)	Controls non-obese (n = 20)	P
Age (years)	44,2 (12,1)	52 (16,4)	0,1
Female:male ratio	31:10	11:9	0,103
Hypertension (n)	16 (39)	5 (25)	0,279
BMI (kg/m2)	48,6 (7,3)	25,4 (3,4)	<0,001
Fasting blood sugar (mg/dL)	97,4 (18,3)	93,3 (13,9)	0,535
Triglycerides (mg/dL)	145,5 (89,8)	117,6 (50,7)	0,311
Insulin (mIU/L)	3,5 (3,3)	2,2 (3)	0,014
HOMA-IR	14,4 (12,6)	8,8 (11)	0,011

Appendix - Supplementary Materials and Methods

Generation of stable cell lines

For long-term gene silencing of PKD1, 3T3L1 cells were transduced using lentivirus with an integrated shRNA, which was ligated into the vector between XhoI and EcoRI cloning sites. pGIPZ shNTC was used as a negative control (shPKD1:

5' tgctgttgacagtgagcgatacagatacagcgaatgtagtgtattatagtgaagccacagatgtataatacactgcctcgga 3'). These sequences were synthesized by Eurofins and cloned into a pGIPZ shRNAmir (generous gift from Eilers lab, Biocenter, Würzburg) as previously described (Fellmann, Hoffmann et al., 2013). Lentivirus was produced by transfection of HEK293T cells with shRNA and the two packaging vectors, psPAX (Adgene) and pMD2.G (Adgene), using Dharmafect Duo (GE Healthcare) according to the manufacturer's instructions. 3T3L1 cells were transduced with the virus supplemented with polyprene (8µg/mL, Sigma-Aldrich) after 24 and 48 hours. Afterwards, cells were selected by puromycin treatment (5µg/mL, Thermo Fischer Scientific) for up to one week. The retroviral pBabe-Puro system (Cell Biolabs) was used for expression of c-terminal Myc-tagged PKD1 wild type and constitutive active form (S744E/S748E). Both coding sequences (generous gift from Ricci lab, IGBMC, Strassbourg) were introduced into the plasmid between BamHI and EcoRI restriction sites. Retroviral particles were produced using Platinum-E cells. Transduction and selection of 3T3L1 was performed according to the lentiviral procedure.

Transient transfection with siRNA

Fully differentiated SVC or 3T3L1 cells were transfected with Dharmafect Duo transfection reagent and siRNA against AMPKα1/AMPKα2 or NonTarget control (GE Healthcare), as well as Cebpα, Cebpδ, and Cebpα/δ as described before (Cai et al., 2017). Experiments were conducted 48 hours post transfection (siPrkaa1 #M-041035-02-0005; siPrkaa2 #M-040809-01-0005; siGENOME Non-Targeting siRNA Pool #1 #D001206-13-05, siCebpa #M-040561-01-0005, siCebpd #M-040561-01-0005).

DAG content

50 mg of tissue was homogenized in 7-fold volume of 1% acetic acid using a stirring plastic pistil. 280 µl of the homogenate, 70 µl methanol, 210 µl n-butanol and 20 µl 10 mM dioctanoylglycerol in n-butanol/methanol (3/1, v/v) were mixed vigorously. After addition of 200 µl n-heptane and 100 µl acetic acid ethylester, the solution was mixed and centrifuged for 2 min at max rpm. The resulting upper phase was transferred to a new tube. The lower phase was extracted with another 200 µl n-heptane and 100 µl acetic acid ethylester. The combined upper phases were evaporated at 45 °C under a stream of N2. Lipid Class Separation: The dried DAG extract was resuspended in 150 µl hexane and applied on a Silica-Matrix Column (Phenomenex, Aschaffenburg, Germany). Undesired lipids were washed out by applying 750 µl hexane, 750 µl hexane/acetic acid ethylester (18/1, v/v) and 1.5 ml hexane/acetic acid ethylester (9/1, v/v) to the column. DAGs were eluted with 750 µl hexane/acetic acid ethylester (9/4, v/v). The eluate was collected and evaporated to dryness at 45 °C under a stream of N2. LC/MS Analysis of DAGs: For LC/MS analysis, the resulting residue was dissolved in 250 µl mobile phase A / mobile phase B (70/30, v/v). Mobile phase A consisted of acetonitrile/water/formic acid (10/89.9/0.1, v/v/v), and mobile phase B consisted of acetonitrile/water/formic acid (90/9.9/0.1, v/v/v). The equipment used for LC/MS analysis was a Thermo Scientific Dionex Ultimate 3000 UHPLC system hyphenated with a Q exactive mass spectrometer (QE-MS) equipped with a HESI probe (Thermo Scientific, Bremen, Germany), and UPLC-column: Acclaim RSLC 120 C8 reversed-phase column (2.2 µm particles, 50 × 2.1 mm) (Thermo Scientific, Bremen, Germany). After injection of 5 µl sample to the C8 column (at 40 °C), the gradient program was: 20% solvent B for 2 min, followed by a linear increase to 100% solvent B within 5 min, then maintaining 100% B for 22 min, then returning to 20% B in 1 min and 5 min 20% solvent B for column equilibration before each injection. The flow rate was maintained at 350 µL/min and the eluent was directed to the ESI source of the QE-MS. MS parameters: Heater temperature, 120 °C; sheath gas, 30; auxiliary gas, 10; sweep gas, 3; spray

voltage, 3.6 kV. Capillary temperature was set at 320 °C, and S-lens was 55. A full scan range from 300 to 700 (m/z) in positive ion mode was used. The resolution was set at 70000. The maximum injection time was 200 ms. Data evaluation: Peak corresponding to the calculated DAG masses (MIM-OH- ± 2 mMU) were integrated using TraceFinder software (Thermo Scientific, Bremen, Germany).

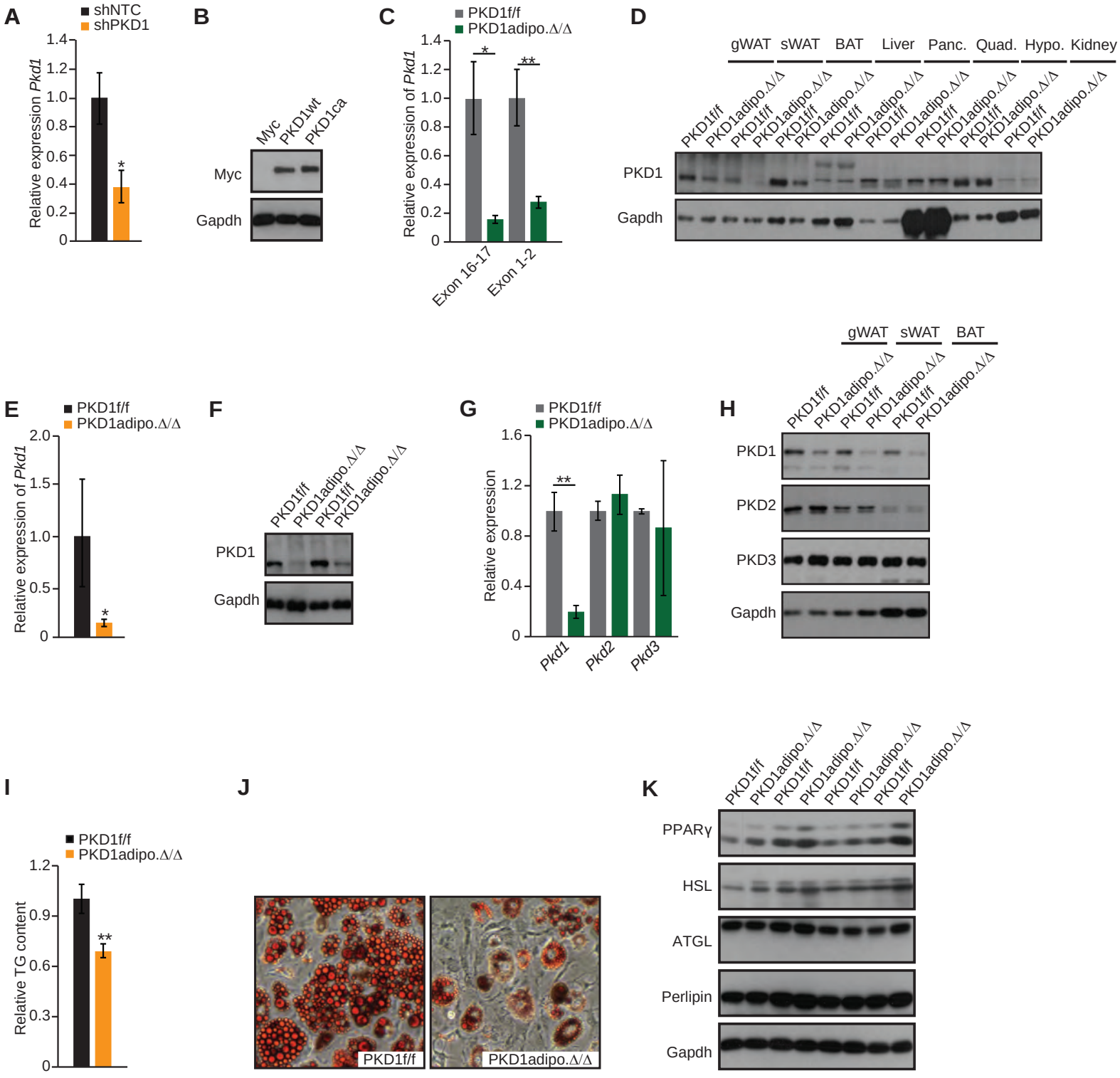

Appendix - Figure S1

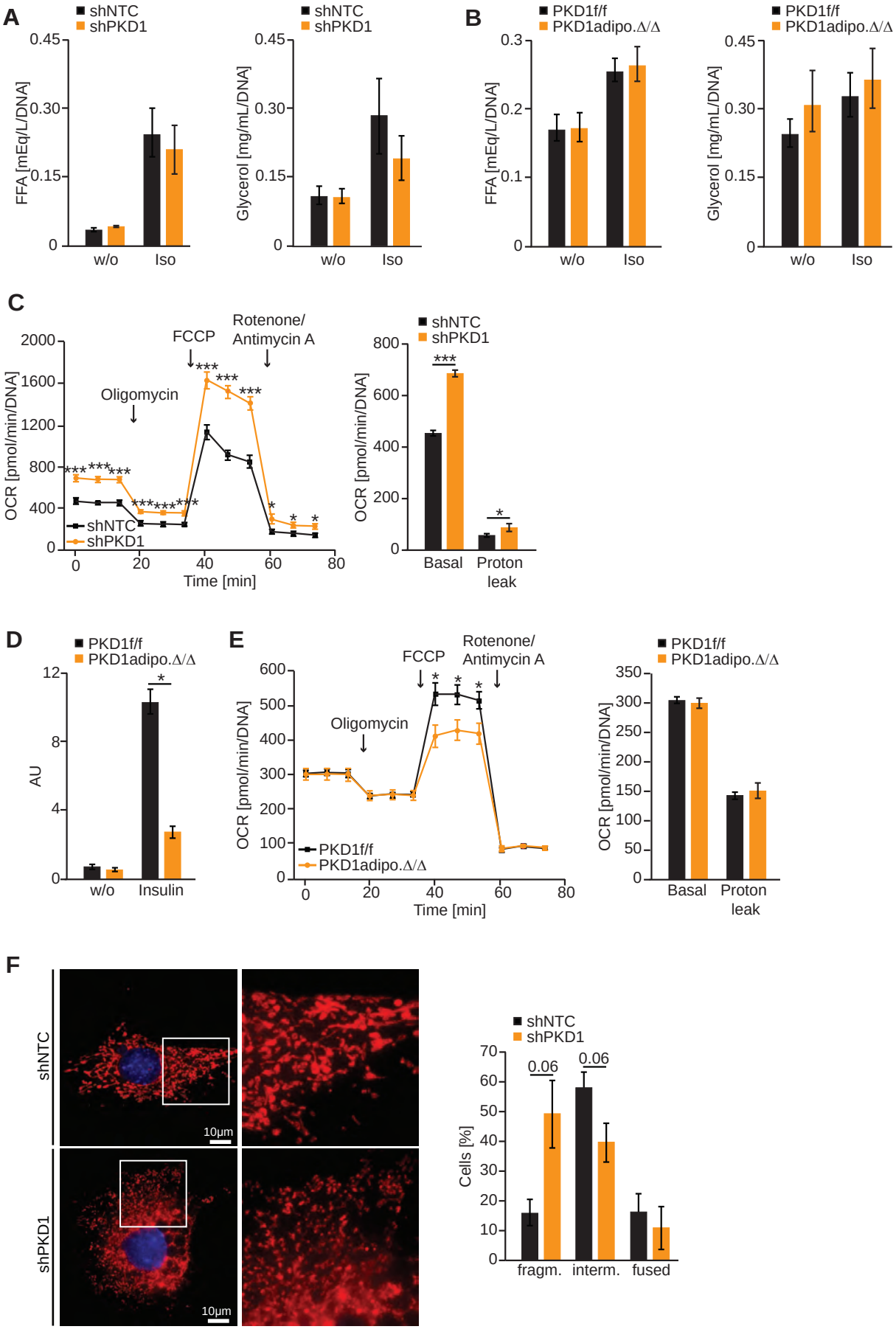

Appendix - Figure S2

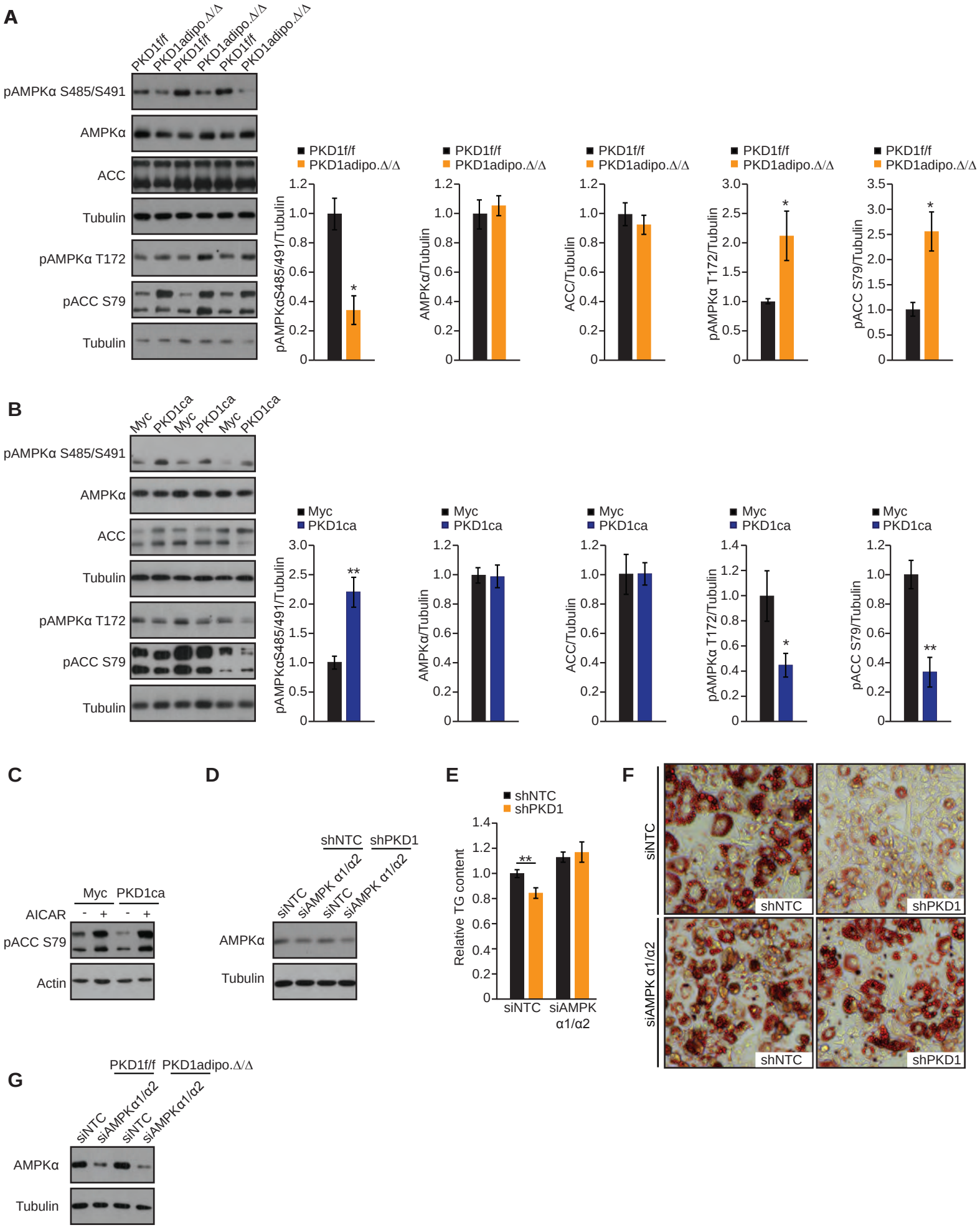

Appendix - Figure S3

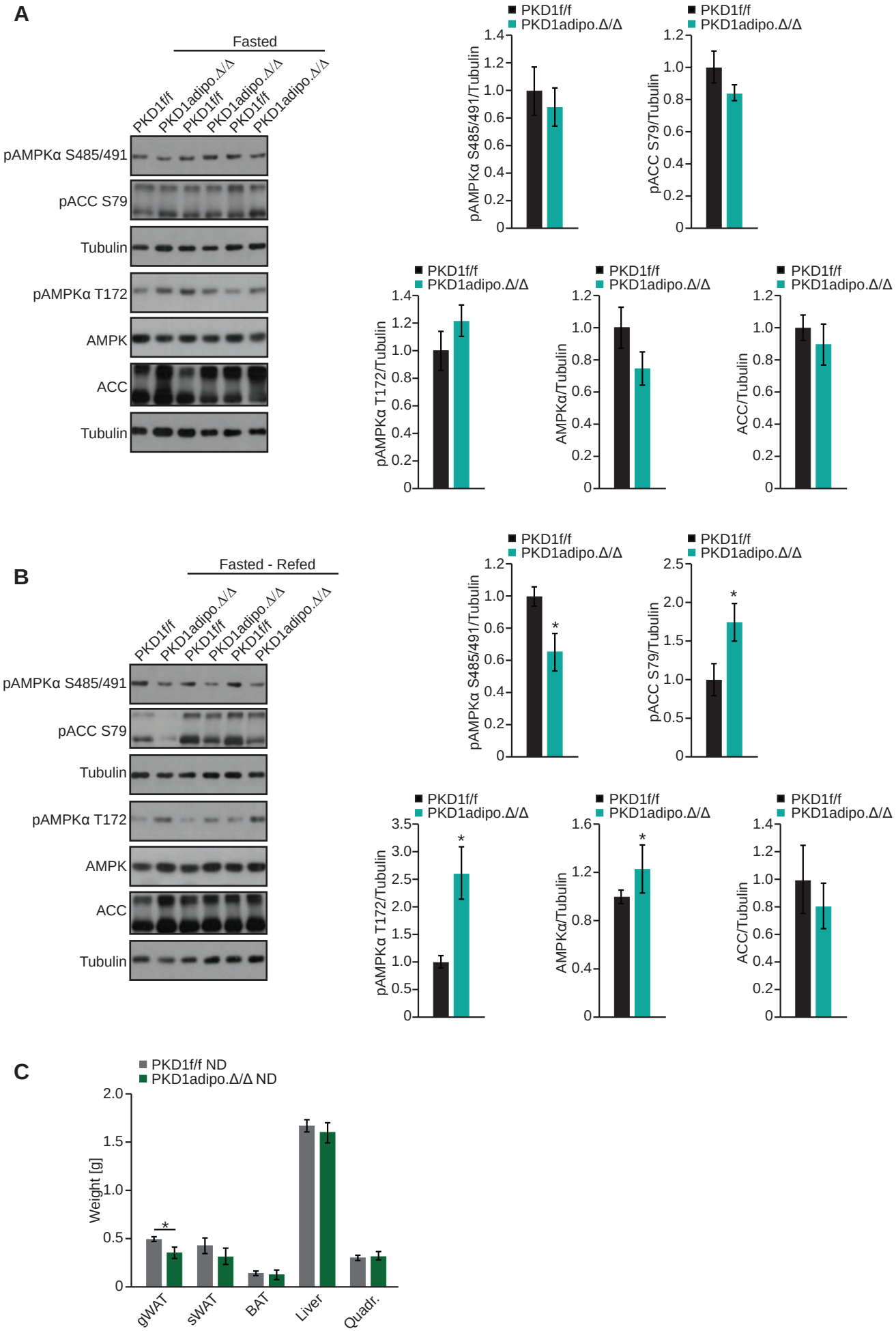

Appendix - Figure S4

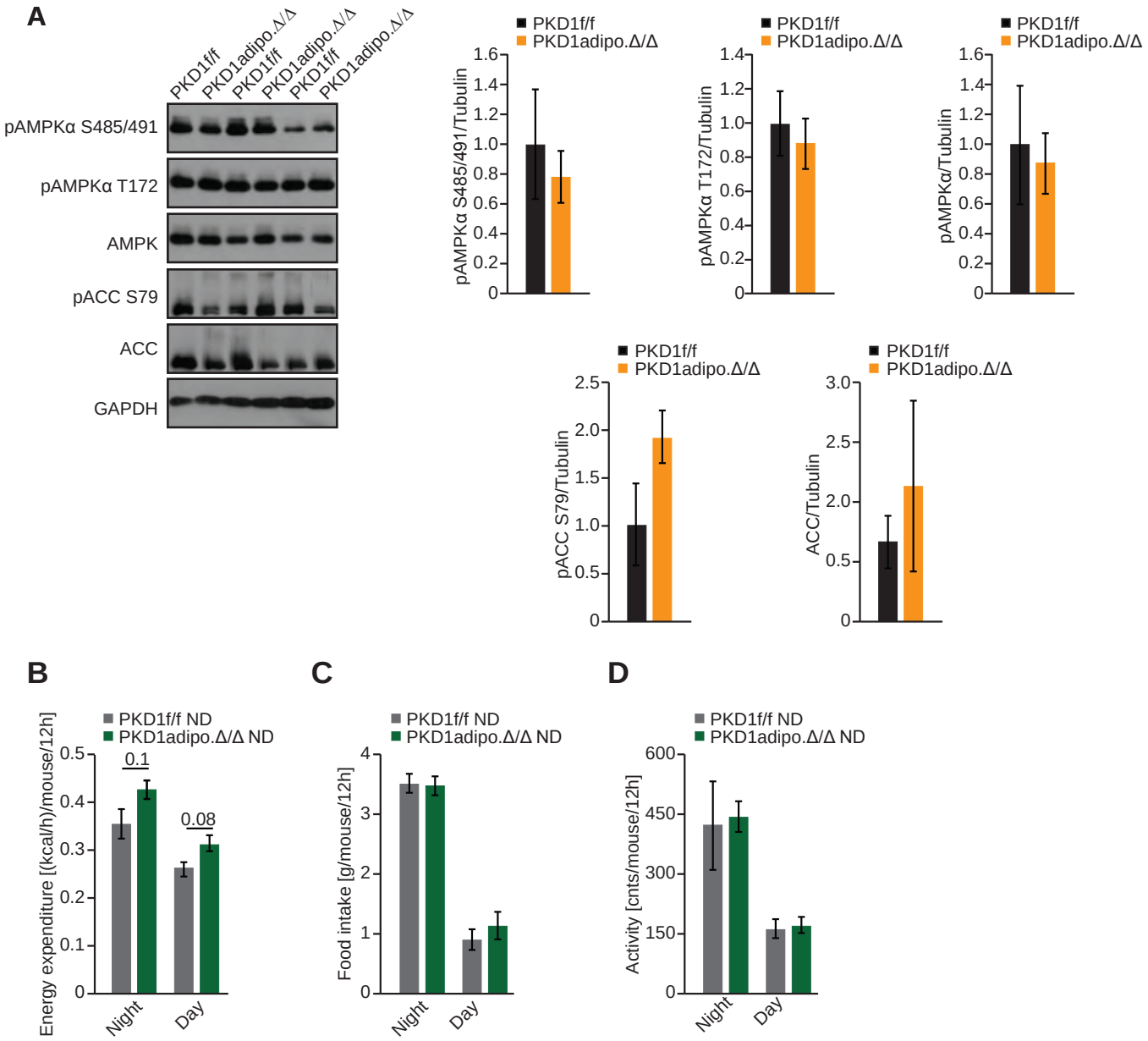

Appendix- Figure S5

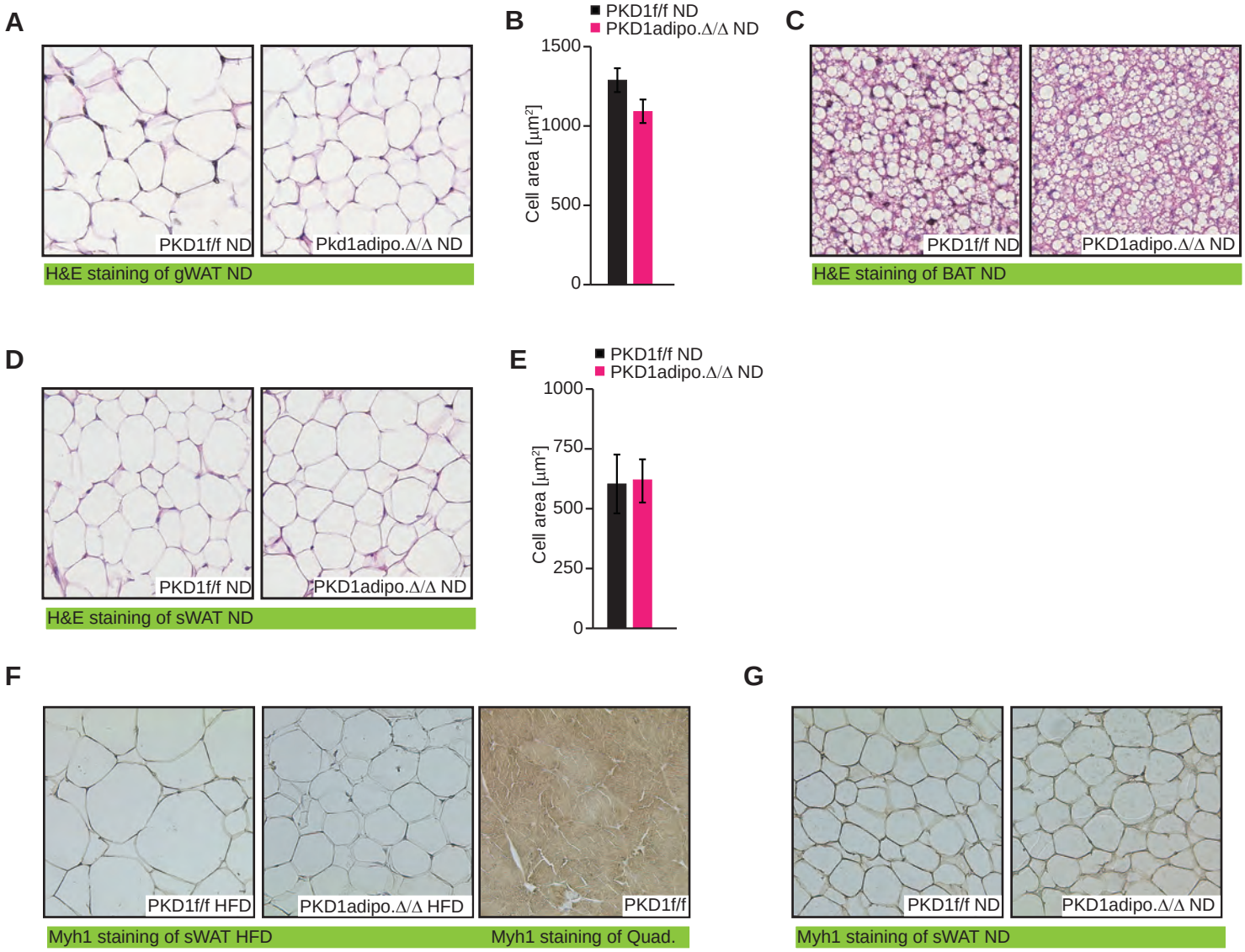

Appendix- Figure S6

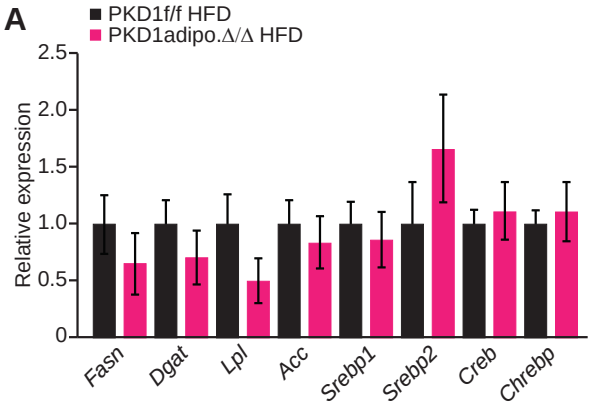

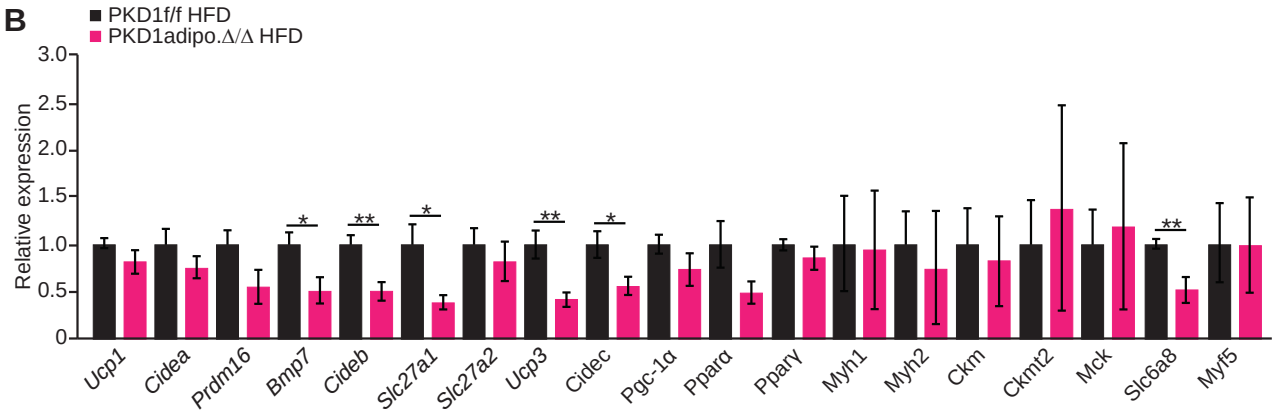

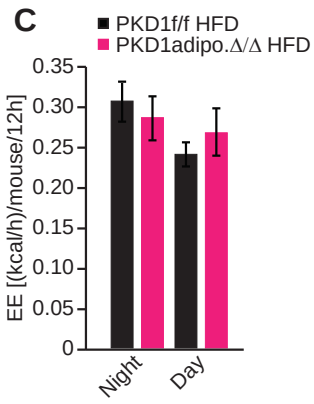

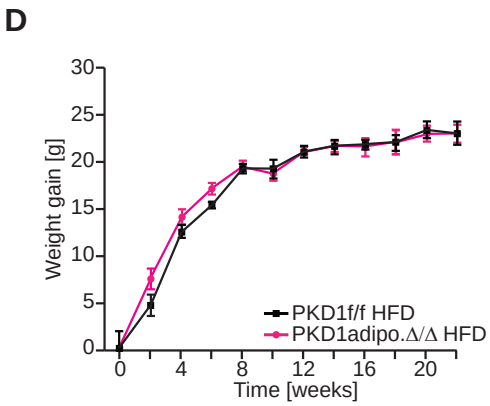

Appendix- Figure S7

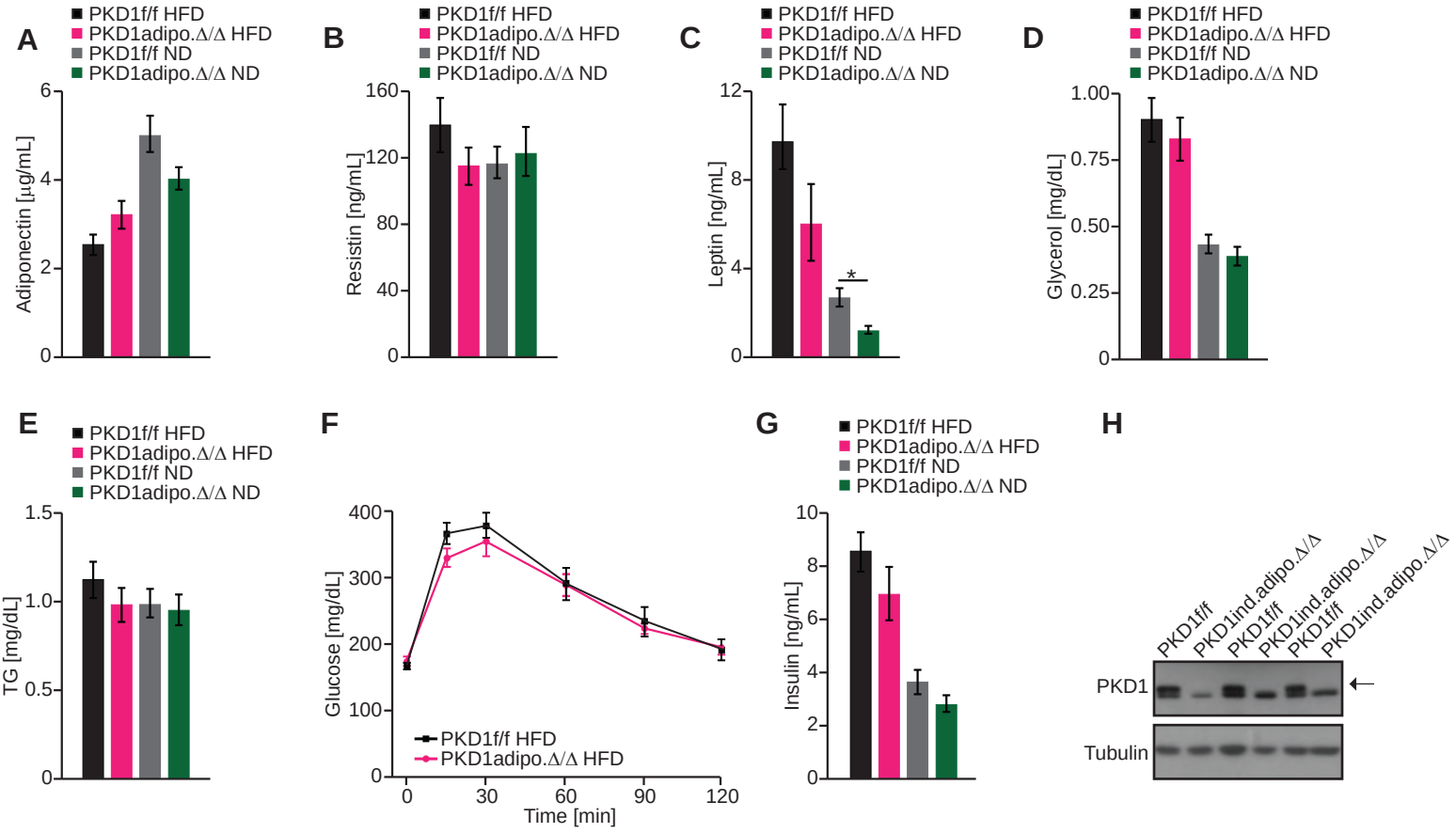

Appendix- Figure S8

Appendix Figure S1 - Deletion of PKD1 does not affect protein levels of markers of adipocyte differentiation.

A. QPCR analysis of *Pkd1* levels in 3T3L1 cells expressing shRNA against PKD1 and control cells (n=4; representative of three different experiments).

B. WB analysis using indicated antibodies in 3T3L1 cells expressing Myc, PKD1wt, and PKD1ca.

C. QPCR analysis of *Pkd1* expression using primers located in exon 16 and 17 as well as exon 1 and 2 of the *Pkd1* gene in adipocytes of PKD1adipoΔ/Δ and control mice (n=4/genotype).

D. WB analysis of PKD1 expression in indicated organs of control and PKD1adipoΔ/Δ mice.

E. mRNA levels of *Pkd1* in SVC-derived adipocytes isolated from PKD1adipoΔ/Δ and control mice (n=4/genotype; representative for three individual experiments).

F. PKD1 levels defined by WB in SVC-derived adipocytes isolated from PKD1adipoΔ/Δ and control mice.

G. QPCR analysis of indicated gene expression in adipocytes of PKD1adipoΔ/Δ and control mice (n=4/genotype).

H. WB analysis of PKD1, PKD2, and PKD3 expression in indicated organs of control and PKD1adipoΔ/Δ mice.

I, J Quantification of relative TG accumulation using AdipoRed reagent (H) and images of Oil-Red-O staining for neutral lipids (I) was performed in PKD1-deficient SVC differentiated into adipocytes (n=3; representative of three individual experiments).

K. WB analysis of expression of indicated proteins in SVC-derived adipocytes isolated from PKD1adipoΔ/Δ and control mice.

Data information: In (A, C, E, G, and I), data are presented as mean ± SEM. *$P < 0.05$ and **$P < 0.01$, (unpaired, two-tailed Student's t-Test).

Appendix Figure S2 - PKD1 promotes lipogenesis in brown adipocytes but does not affect their energy dissipation.

A. FFAs and glycerol secretion from control and PKD1-depleted 3T3L1 cells stimulated with vehicle or Iso (10 μM) (n=6; representative for three individual experiments).

B. FFA and glycerol secretion in unstimulated or 10 μM isoproterenol (Iso.) stimulated adipocytes derived from SVC isolated from mice of indicated genotypes (n=6/genotype; representative for three individual experiments).

C. OCR in response to the indicated substances and OCR annotated to the indicated substances in differentiated 3T3L1 cells lacking PKD1 (n=14; representative of three individual experiments).

D, E Lipogenesis rate (D) and OCR in response to the indicated substances as well as OCR annotated to the indicated substances (E) in differentiated brown adipose tissue stromal-vascular cells (BSVC) derived from mice of indicated genotypes (in D, n=3; in E, n=26; representative of two individual experiments).

F. Representative microscopy images of the mitochondrial morphology and its respective quantification in differentiated PKD1-deficient 3T3L1 cells.

Data information: In (A-F), data are presented as mean ± SEM. In (F), data represent three independent experiments with 200 cells counted for each replicate. *P < 0.05 and ***P < 0.001 (unpaired, two-tailed Student's t-Test).

Appendix Figure S3 - PKD1 deletion in adipocytes suppresses TG accumulation in an AMPK-dependent manner.

A, B WB analysis using antibodies against indicated proteins in lysates of differentiated PKD1-deficient SVC (A) and 3T3-L1 cells expressing PKD1ca (B) and densitometric quantification of up to 4 replicates for each protein (A, B).

C, D WB analysis using indicated antibodies in 3T3L1 cells expressing PKD1ca treated with AICAR (2 mM) for 2 hours (C) and differentiated 3T3L1 cells lacking PKD1, which have been transfected with siRNA against AMPKα1/α2 (D).

E, F Quantification of relative TG accumulation using AdipoRed reagent (E) and images of Oil-Red-O staining for neutral lipids (G) in differentiated 3T3L1 cells lacking PKD1 which have been transfected with siRNA against AMPKα1/α2 (n=3; representative of three individual experiments).

G. WB analysis of indicated proteins in differentiated SVC transfected with control siRNA and siRNA against AMPKα1/α2.

Data information: In (A, B, and E), data are presented as mean ± SEM. *P < 0.05 and **P < 0.01 (unpaired, two-tailed Student's t-Test).

Appendix Figure S4 - PKD1 deletion enhances AMPK signaling in adipose tissue of fasted-refed mice.

A, B WB analysis of indicated proteins in sWAT of control and PKD1-deficient mice, which have been fasted for 24 hours (A) or 24 hours fasted followed by 24 hours refeeding (B) including densitometric quantification of 5 replicates each (A, B).

C. Weight of indicated organs in PKD1adipoΔ/Δ and control mice fed ND (n>5/genotype).

Data information: In (A-C), data are presented as mean ± SEM. *P < 0.05 (unpaired, two-tailed Student's t-Test).

Appendix Figure S5 - PKD1 deletion in adipocytes has only minor effects on metabolism of mice fed ND.

A. WB analysis of indicated proteins in differentiated SVC derived from BAT of control and PKD1-deficient mice including densitometric quantification of triplicates each.

B-D Energy expenditure (B), food intake (C), and voluntary movement (D) of PKD1adipoΔ/Δ and control mice fed ND (n>5/genotype).

Data information: In (A-D), data are presented as mean ± SEM (unpaired, two-tailed Student's t-Test.

Appendix Figure S6 - PKD1 deletion in adipocytes of mice fed ND does not change adipocyte size.

A-E Representative H&E stainings of gWAT (A), BAT (C), and sWAT (D) from PKD1adipoΔ/Δ and control mice fed ND. Average adipocytes size in gWAT (B) and sWAT (E) of indicated mice (n>5/genotype).

F, G Myosin heavy chain1 (Myh1) stainings of sWAT from PKD1adipoΔ/Δ and control mice fed HFD and ND (n=4/genotype). Quadriceps sample of a wild-type mouse has been included as a positive control.

Data information: In (B, E), data are presented as mean ± SEM (unpaired, two-tailed Student's t-Test).

Appendix Figure S7 - PKD1 does not suppresses expression of thermogenesis-related genes in BAT.

A, B QPCR analysis of indicated gene expression in sWAT (A) and BAT (B) from PKD1adipoΔ/Δ and control mice fed HFD (n=6/genotype).

C, D Energy expenditure (C) and body weight gain (D) of control and PKD1adipoΔ/Δ mice fed HFD and housed under thermoneutral (30°C) conditions (n>6/genotype).

Data information: In (A-D), data are presented as mean ± SEM. *$P < 0.05$ and **$P < 0.01$ (unpaired, two-tailed Student's t-Test).

Appendix Figure S8 - PKD1 deletion in adipocytes results in reduced leptin levels.

A-F Adiponectin (A), resistin (B), leptin (C), glycerol (D), and TG (E) levels in serum of PKD1adipoΔ/Δ and control mice fed ND and HFD (n>5/genotype).

F. Glucose tolerance test of control and PKD1-deficient mice after 8 weeks of HFD feeding (n>8/genotype)

G. Insulin levels in blood of PKD1adipoΔ/Δ and control mice fed ND and HFD (n>5/genotype).

H. WB analysis of PKD1 protein in control and tamoxifen-inducible PKD1-deficient mice.

Data information: In (A-G), data are presented as mean ± SEM. *P < 0.05 (one way ANOVA with Tukey's multiple comparisons post test (A-E, and G) or unpaired, two-tailed Student's t-Test (F)).